Chapter 4
Functional analysis of G2

4.1 Manipulation of G2 Expression

The expression analysis described in chapter 3 indicates that *G2* is expressed specifically in AZ and in cortical cells overlying the lateral root primordial. The approach that was applied to determine the function of G2 was to manipulate its expression. A reverse genetics strategy was applied to investigate the role of *G2* in plant development.

Two T-DNA insertion lines associated with *G2* were identified and seeds were obtained from Nottingham *Arabidopsis* Stock Centre (NASC). Homozygous knock out lines were determined by PCR. Unfortunately none of them showed a reduction in expression of *G2* in floral tissues. An RNAi strategy was then undertaken and homozygous lines were isolated and the phenotypes of down-regulated lines were studied.

To further investigate the potential function of *G2*, the gene was ectopically expressed under the regulation of a 35SCaMV promoter. The resulting *G2* ectopic expression lines were characterized in detail.

4.1.1. Generation of *G2* null lines using a T-DNA strategy

A T-DNA insertion strategy was applied to generate null lines of *G2*. T3 T-DNA insertion lines SALK_065404 and SALK_055356 (Figure 4.1) were identified and obtained from NASC (European *Arabidopsis* Stock Centre) (Scholl RL, *et al.*, 2000). The T-DNA insertions were at 310 bp (SALK_065404) and 360 bp (SALK_055356) upstream of the translation start site. Genomic PCR was used to identify the homozygous KOs of the two T-DNA insertion lines (Figure 4.1).
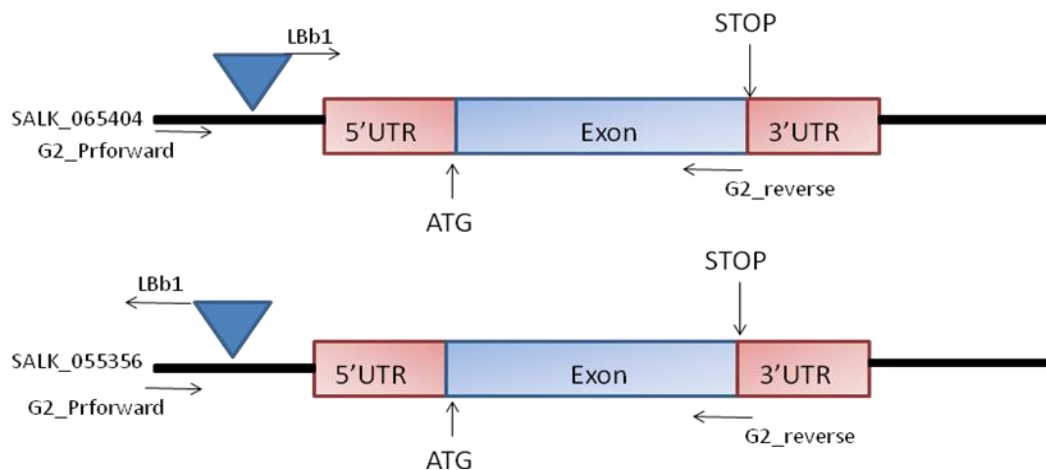

Figure 4.1 A schematic diagram of T-DNA insertion positions of *G2*. The diagrams are not drawn to scale.

For T-DNA insertion line SALK_065404, the genomic PCR result indicates that samples 3 and 6 are the T-DNA insertion homozygotes (Figure 4.2) (Shahid, unpubished data).
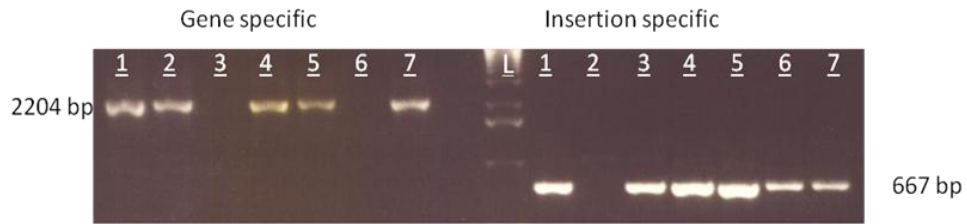
Figure 4.2 PCR analysis of putative T-DNA insertion lines (SALK_565404) of *G2*. Group Insertion specific shows the PCR products amplified by primers LBb1 and G2_reverse (Table 1.1). Group Gene Specific shows the PCR products amplified by primers G2PR_Forward & G2_reverse. L: ladder. Lines 3 and 6 were identified as homozygous insertion lines.

For T-DNA insertion line SALK_055356, the PCR result indicates that sample 1, 2, and 4 are the T-DNA insertion homozygotes (Figure 4.3).
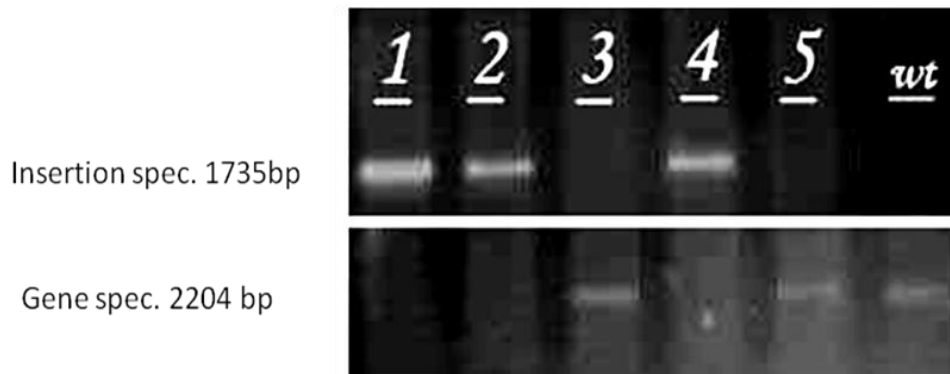
Figure 4.3 PCR analysis of putative T-DNA insertion lines (SALK_55356) of *G2*. Group Insertion specific shows the PCR products amplified by primers G2PR_F & LBb1. Group Gene Specific shows the PCR products amplified by primers G2PR_F & G2_rev. wt: wild type. Lines 1, 2 and 4 are identified as homozygous insertion lines.

A Reverse-transcription PCR (RTPCR) was then carried out to confirm that *G2* expression was silenced in the KO lines. Total RNA was isolated from flowers in position 5 – 8. HK-CBP primers (Table 1.1) were used to amplify

housekeeping transcripts. The results showed that neither of the T-DNA insertion lines exhibited reduced the expression of G2 (Figure 4.4).
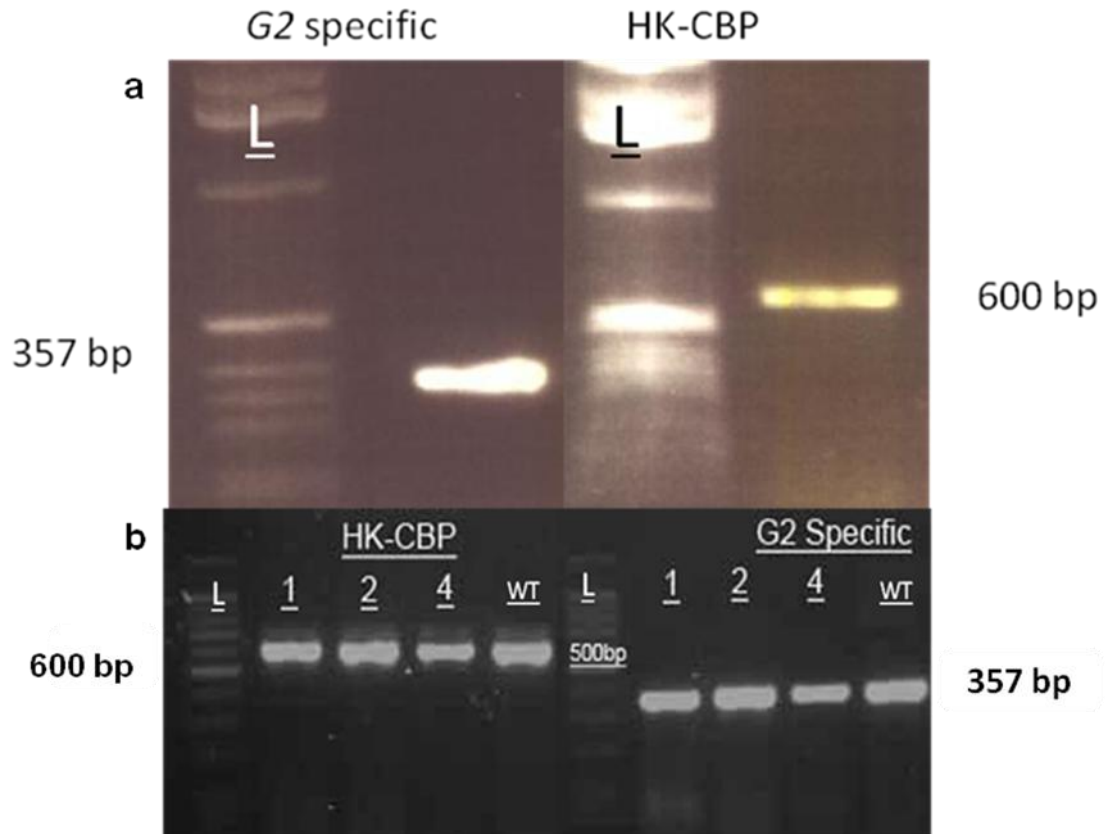

Figure 4.4 RT-PCR analysis of putative T-DNA insertion lines, SALK_65404 and SALK_055356. Group HK-CBP shows the RT-PCR product amplified by HK-CBP primers and group G2 Specific shows the RT-PCR product amplified by G2_Forward and G2_Reverse primers. L: ladder.

4.1.2. Generation of *G2* null lines using an RNAi strategy

Fragments with 357 base pairs covering the full length cDNA of *G2*, were fused into an entry vector pDONR221 (Invitrogen™) by using a Gateway™ Technology (Figure 4.5). Because the gene does not have an intron,

primers with attB1.1 and attB2.1 sites (Table 1.1) were designed and the amplified fragments from PCR by using Phusion™ DNA Polymerase were purified before fusing them into the vector pDONR221 by the Gateway™ BP-reaction strategy which was described in section 2.2.10. The resulting construct was called G2Entry (Figure 4.6). The plasmids were then transformed into *E.coli* strain DH5α using a heat-shock method (Sambrook *et al.,* 1989) as described in section 2.2.8**.** The transformed cells were selected by spreading the cells on LB medium plates containing 50 µg/ml kanamycin and the resistant plasmids were isolated and purified using a NucleoSpin™ Plasmid mini kit which has been described in section 2.2.9. The plasmids were confirmed by PCR (Figure 4.7) and then sent for sequencing.
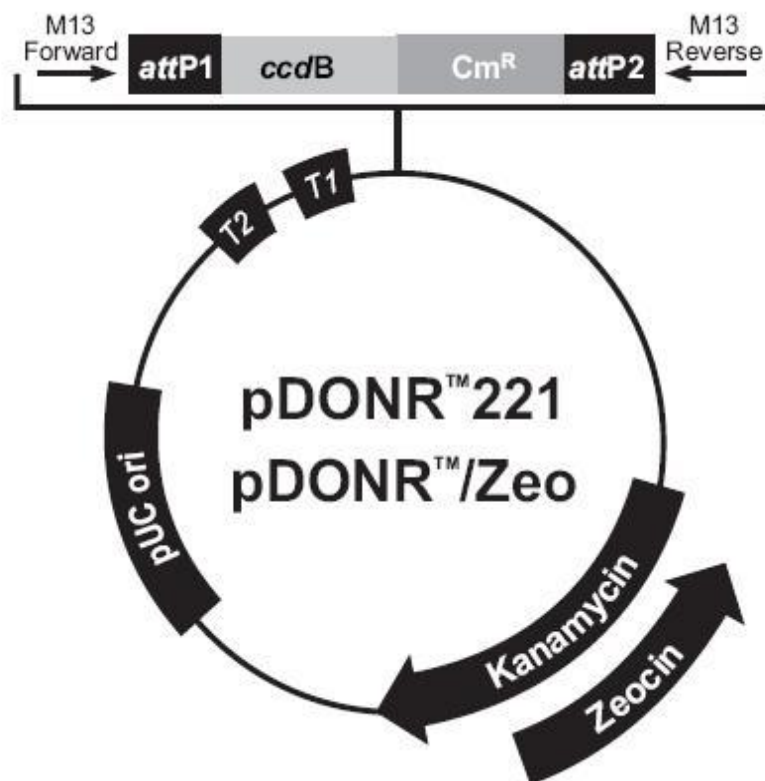
Figure 4.5 Diagram of GateWay™ pDONR™221 entry vector, which contains a pUC origin, a Kanamycin gene, and M13 primers sites for sequencing (Invitrogen™).
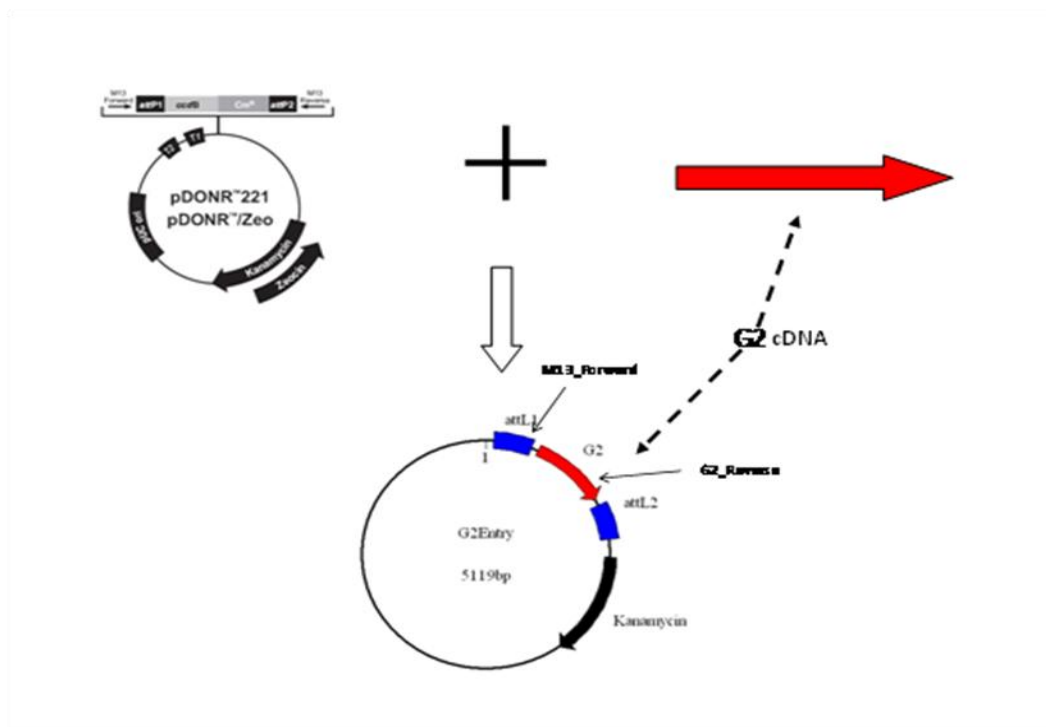
**Figure 4.6** Schematic diagram of G2Entry plasmid construct. The 357 bp *G2* cDNA insert was fused into pDONR™221 by BP reaction. A kanamycin-resistance gene was used as a selectable marker in bacteria.


Figure 4.7 PCR analysis of the colonies that contain the G2Entry plasmid using primers M13_Forward and G2_reverse (Table 1.1). The positions of the primers are shown in figure 4.6. L: ladder.

The RNAi construct was then made by fusing the fragments into a destination vector pK7GWIWG2 which has been described by Karimi *et al* (2005)*.* The Gateway™ technology LR reaction was applied following the procedure described in section 2.2.10. The final construct was named *RNAi:G2*. A diagrammatic representation of the construct is shown in Figure 4.8. Prior to the transformation, the constructs both in *E.coli* DH5α and *Agrobacterium tumefaciens* C58 were confirmed by PCR using respective primers (Table 1.1). DNA bands with the expected size were successfully amplified (Figure 4.9).
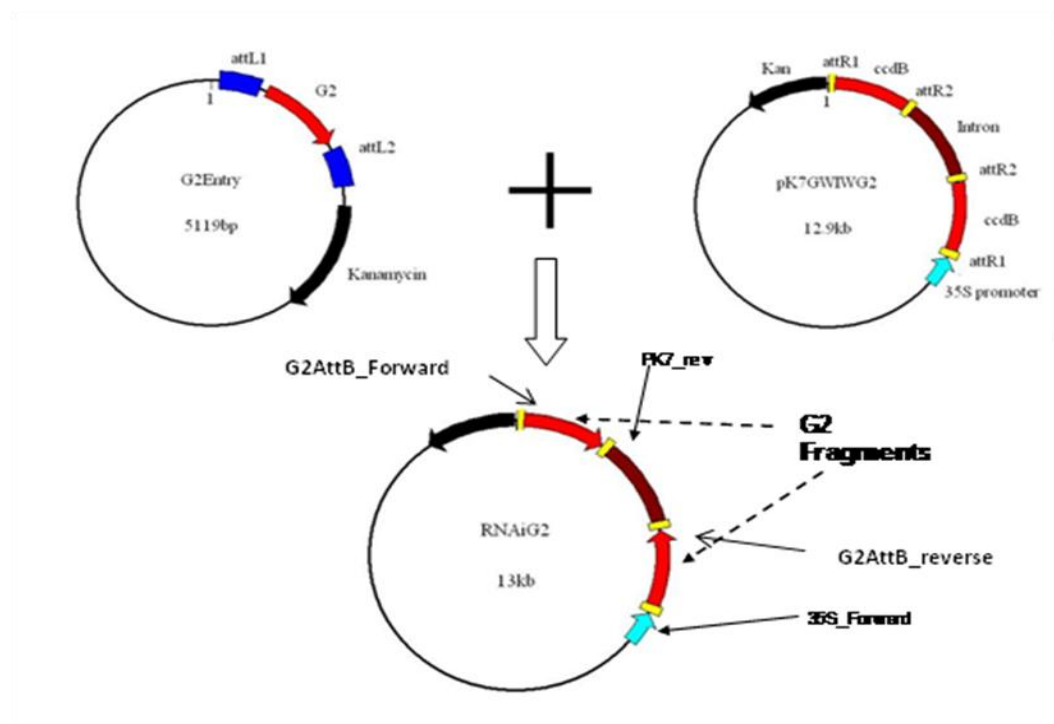
Figure 4.8 The *G2* cDNA fragment in the Entry Clone was transferred to a destination vector, pK7GWIWG2, which contains compatible recombination sites, *att*R1 and *Att*R2, in a reaction mediated by Gateway™ LR Clonase™ Enzyme Mix (Invitrogen). The resulting construct was named *RNAI:G2*. This construct was expected to produce hairpin RNA from the inserted G2 fragments, triggering post-transcriptional gene silencing. The diagrams are not drawn to scale.
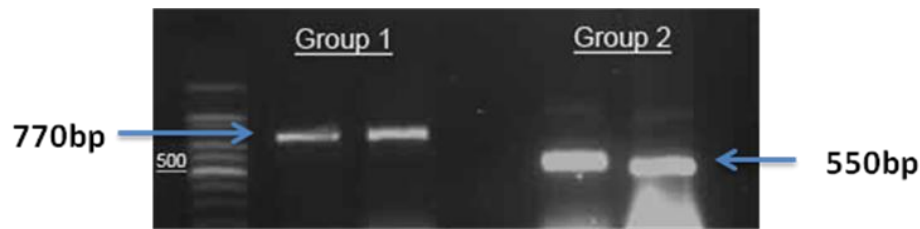
Figure 4.9 PCR analysis of plasmids from the two colonies transformed with *Agrobacterium tumefaciens* C58. **Group1** shows the PCR products amplified by primers G2AttB_forward & PK7_Reverse (Table 1.1). **Group2** shows the PCR products amplified by primers 35S_Forward & G2AttB_reverse. The positions of primers are shown in Figure 4.8.

The plasmid carrying constructs *RNAi:G2* in *Agrobacterium tumefaciens* C58 were transformed into *Arabidopsis thaliana* flowers by the "Floral dip method" (Clough and Bent, 1998) which has been described in section 2.2.12. A total of 14 independent primary transformants for *RNAi:G2* were obtained from the Kanamycin-resistant screening. In order to confirm the down-regulation of *G2* expression, an RT-PCR was carried out by using G2_forward and G2_reverse primers with HK-CBP primers as global control (Table 1.1). Total RNA was isolated from flowers at positions from 5 – 8 where *G2* has the highest amount of expression. Compared to wild type, weak or no RT-PCR product was observed. Two lines without any observed band were selected to generate T2 and T3 to select homozygotes (Figure 4.10).
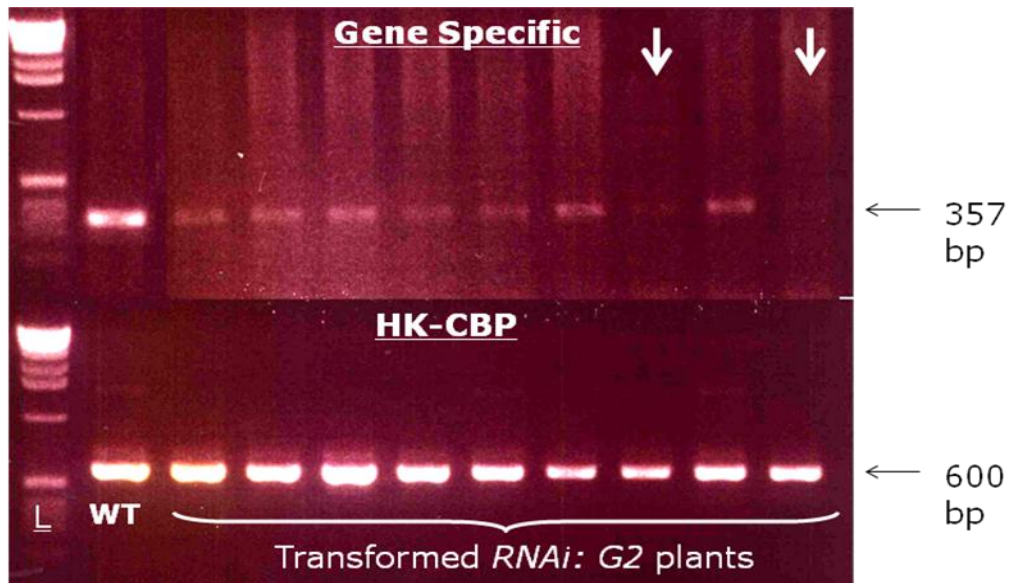
Figure 4.10 RT-PCR analysis of *RNAi:G2* Plants. Group Gene Specific shows the RT-PCR product amplified by using primer G2_Forward and G2_Reverse. Group HK-CBP shows the RT-PCR product amplified using HK-CBP primers. Total RNA was isolated from mature flowers (P5 - 8) of both wild type and primary transformants of *RNAi:G2.* L: ladder.

4.1.3. Generation of ectopically expressing lines of *G2*

The next strategy was to generate overexpression lines of *G2*. The full length cDNA (357 bp) of the gene was inserted into a destination vector pGWB8 which was described in section 2.1.2. The Gateway™ technology LR reaction was then carried out following the procedure described in section 2.2.10. To confirm that transformation was successful, a genomic PCR was carried out using 35S_forward primer and *G2*_reverse primer (Table 1.1) and a band with expected size was obtained. The final construct was named *35S:G2*. A diagrammatic representation of the construct is

shown in Figure 4.11. Prior to the transformation, the constructs both in *E.coli* DH5α and *Agrobacterium tumefaciens* C58 were confirmed by PCR using specific primers. Bands of the expected size were successfully amplified (Figure 4.12).
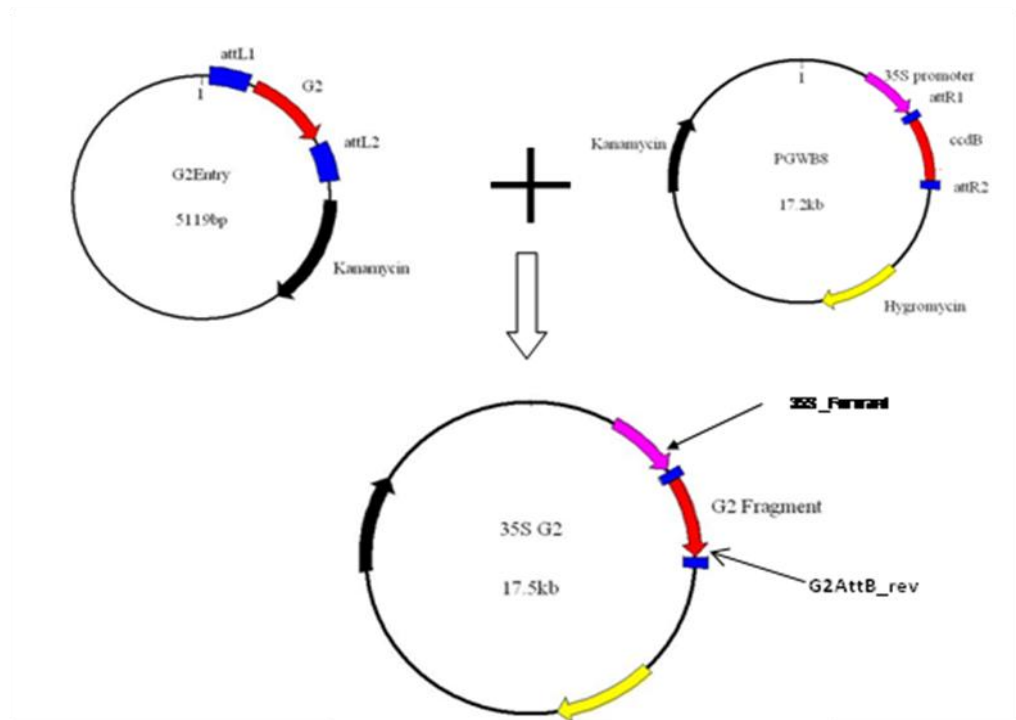
**Figure 4.11.** The G2 fragment in the Entry Clone was transferred to a destination vector, pGWB8, which contains compatible recombination sites, *att*R1 and *Att*R2, in a reaction mediated by Gateway™ LR Clonase™ Enzyme Mix (Invitrogen). The resulting construct was named *35S:G2*. This construct is expected to make G2 express intensively in the transformed plants. The diagrams are not drawn to scale.

Figure 4.12 PCR analysis of plasmids from the six colonies of transformed *Agrobacterium tumefaciens* C58. C: Control group from the plasmid transformed into *Agrobacterium tumefaciens* C58. L: ladder. PCR products were amplified using primers 35S_Forward & G2AttB_rev. The position of primers is shown in Figure 4.11.

The plasmid constructs in *Agrobacterium tumefaciens* C58 were transformed into *Arabidopsis thaliana* flowers by the Floral dip method (Clough and Bent, 1998) which has been described in section 2.2.12. The primary transformants of *35S:G2* construct were screened from Kanamycin-resistant screening. A total of 12 independent transformants for *35S:G2* were obtained and transferred into pots containing Levington M3 compost. The T1 transformants were confirmed by genomic PCR using 35S_forward and G2_reverse primers (Table 1.1). In order to confirm the ectopic expression of *G2*, an RT-PCR analysis was carried out using G2_forward and G2_reverse primers (Table 1.1), with HK-CBP primers as global control. Total RNA was isolated from cauline leaves, where G2 does not naturally express. RT-PCR amplification was clearly observed in all the 12 T1 transformants (Figure 4.13). T2 homozygotes were selected by screening T3 progenies in MS media with Kanamycin and 100% resistant lines were considered as homozygotes.
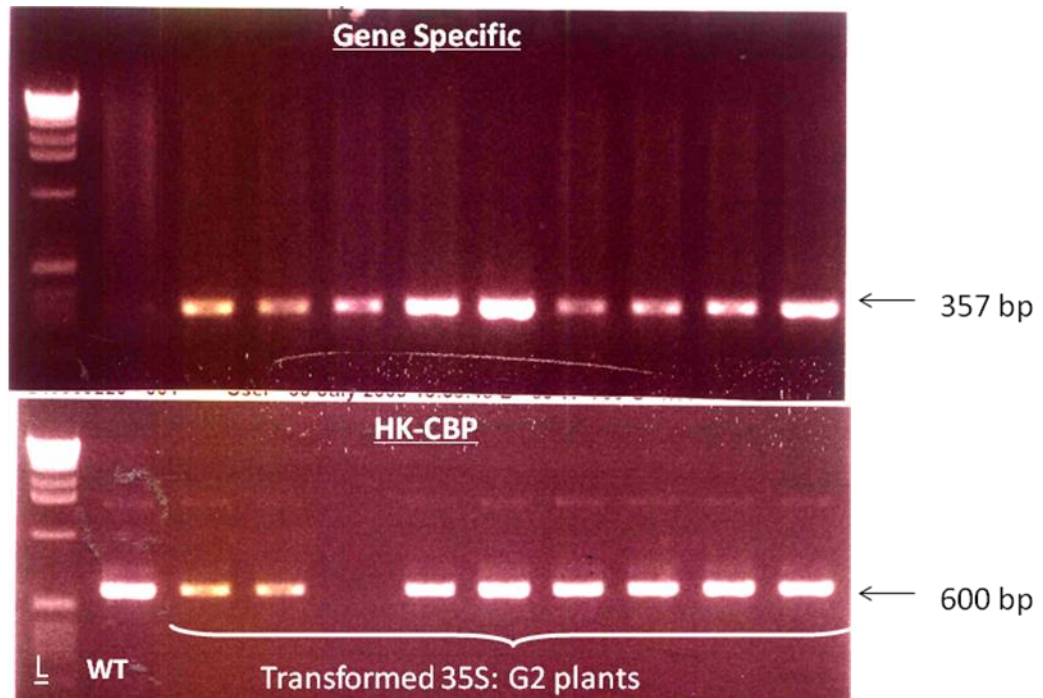
Figure 4.13 RT-PCR analysis of *35S:G2* Plants. Group Gene Specific shows the RT-PCR product amplified using primer G2_Forward and G2_Reverse. Group HK-CBP shows the RT-PCR product amplified using HK-CBP primers. Total RNA was isolated from cauline leaves of mature *Arabidopsis* both wild type and *35S:G2* plants. No expression of *G2* was observed in wild type (WT) comparing to significant expression in Transformed *35S:G2* plants. L: ladder.

4.2 Characterization of Knock Out and overexpression lines of G2 and analysis of phenotypes
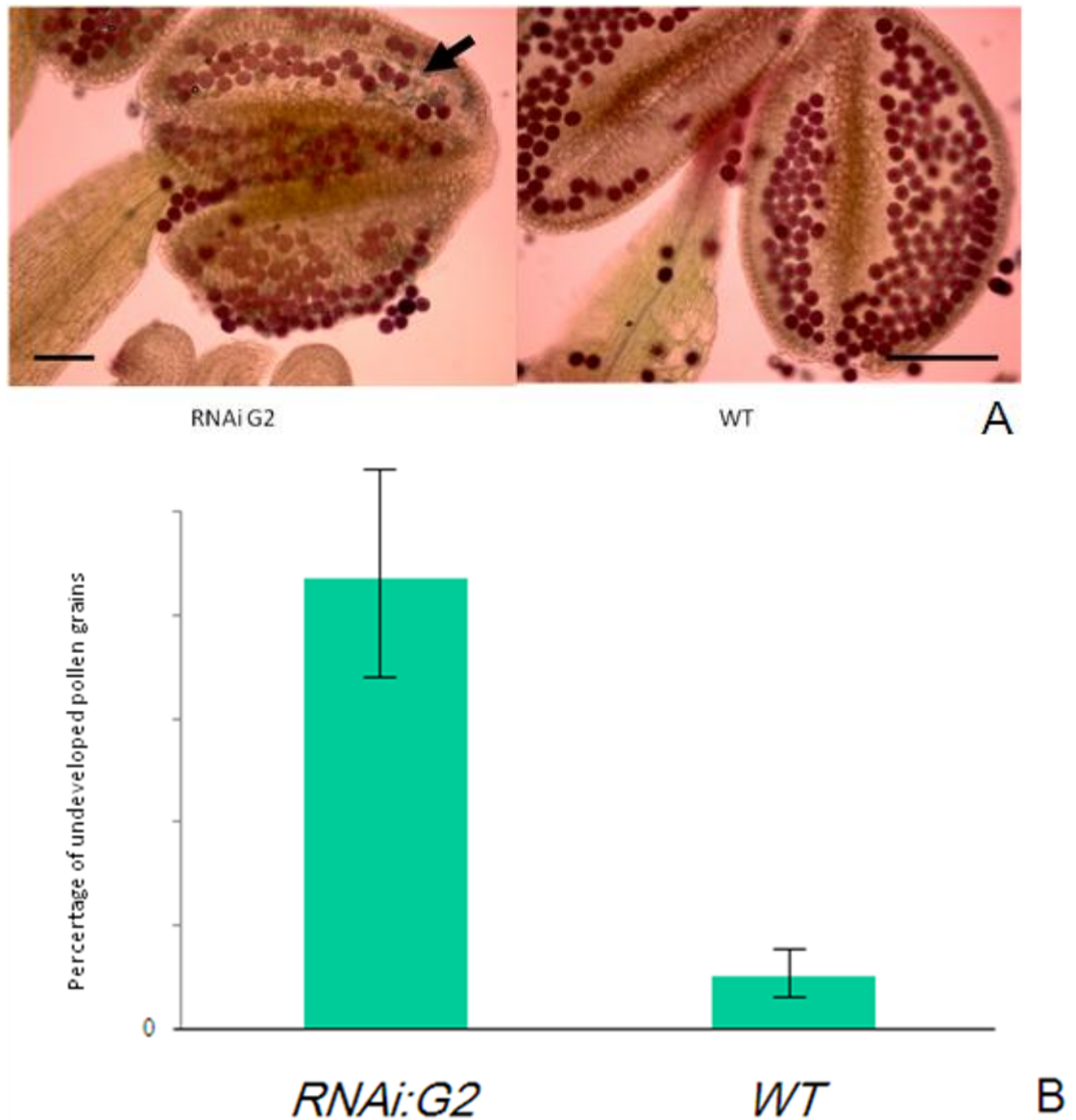
4.2.1 Phenotypes of *RNAi:G2* plants

An in-depth comparative analysis of floral organ abscission was carried out between *RNAi:G2* homozygous and wild type plants. *RNAi:G2* lines did not show any visible difference in either the timing of abscission or in the development of floral organs.

An analysis of pod development in *RNAi:G2* plants revealed that seeds in mature siliques did not all fully develop (Figure 4.14. A, B). Figure 4.14 (C) shows the percentage of normally developed seeds in a wild type and *RNAi:G2* plants. Fourteen pods at position 12 were collected from three individuals of wild type and *RNAi:G2* plants respectively and the percentage of fully developed seeds was calculated. The average final percentage of fully developed seeds in wild type plants was 92% whereas in *RNAi:G2* it was 25%. The abnormal seeds were observed to have aborted.
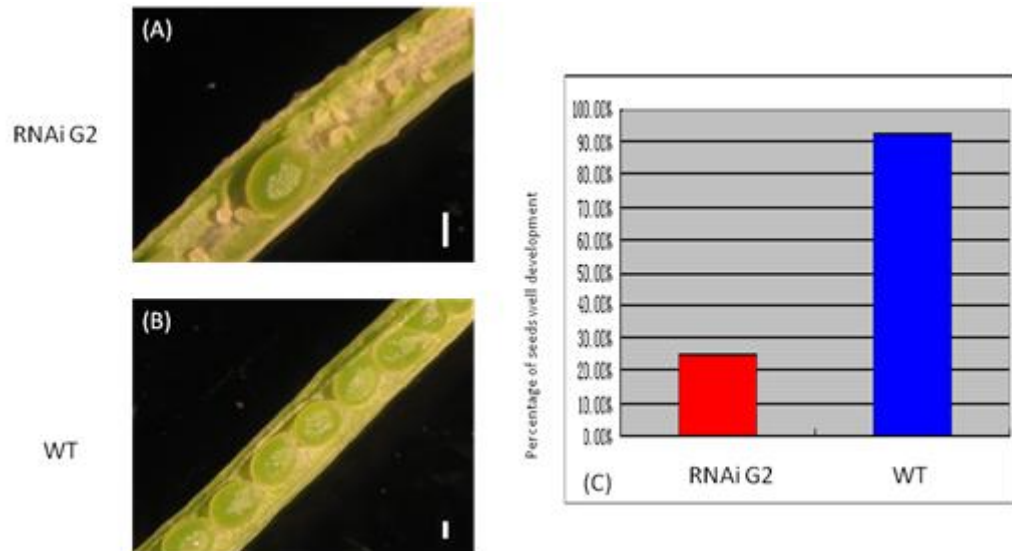
Figure 4.14 Undeveloped seeds identified in siliques of RNAi:G2 **(A)** and wild type **(B)** and the percentage of fully developed seeds **(C).** Scale bar: 100 µm.

A pollen viability test was performed using Alexander staining to determine the viability of the *RNAi:G2* pollen. Pollen grains stained in purple indicate viable cytoplasm, whereas undeveloped pollen is stained green. In comparison to wild type, *RNAi:G2* pollen was only partially functional (Figure 4.15). The percentage of undeveloped pollen per anther was determined by calculating the undeveloped pollen in twenty anthers. The result showed that the average percentage of undeveloped pollen was 21.78%, comparing to 2.45% in wild type.

Picture 4.15 A: Pollen of *RNAi:G2* and wild type stained with Alexander solution. The arrow shows the percentage of undeveloped pollen grains. Scale bar: 50 µm **B**: The percentage of undeveloped pollen grainsRNAi:G2 plant and wild type (WT). Error bars: standard error.

4.2.2 Phenotype of *35S:G2* plants

A phenotypic characterization was carried out in *35S:G2* homozygous lines and wild type plants. The *35S:G2* and wild type plants were grown under the identical conditions as described in section 2.1.1.

An in-depth comparative analysis of floral organ abscission was carried out between *35S:G2* homozygous and wild type plants. The first flower on the inflorescence with visible white petals was considered as position 1. The wild type *Arabidopsis* plant normally abscises its floral organs at position 5 – 7 in natural conditions. Compared to wild type, *35S:G2* lines did not show any significant difference either in the timing of abscission or in the development of floral organs.

An analysis of root development in *35S:G2* seedlings in different stages under the microscope revealed a striking phenotype in root hair development compared to wild type plants. In general the *35S:G2* plants developed significantly shorten and more swollen root hairs. The swollen root hairs were observed as the primary roots emerged from the germinating seeds and this phenotype was maintained throughout root development. However the level of the bulging was observed to be reduced as it came near to the elongation zone. The bulging was observed in trichoblasts and not all the trichoblasts were affected. In some 10-day-old seedlings, the development of root hairs near the elongation zone was indistinguishable to wild type (Figure 4.16).
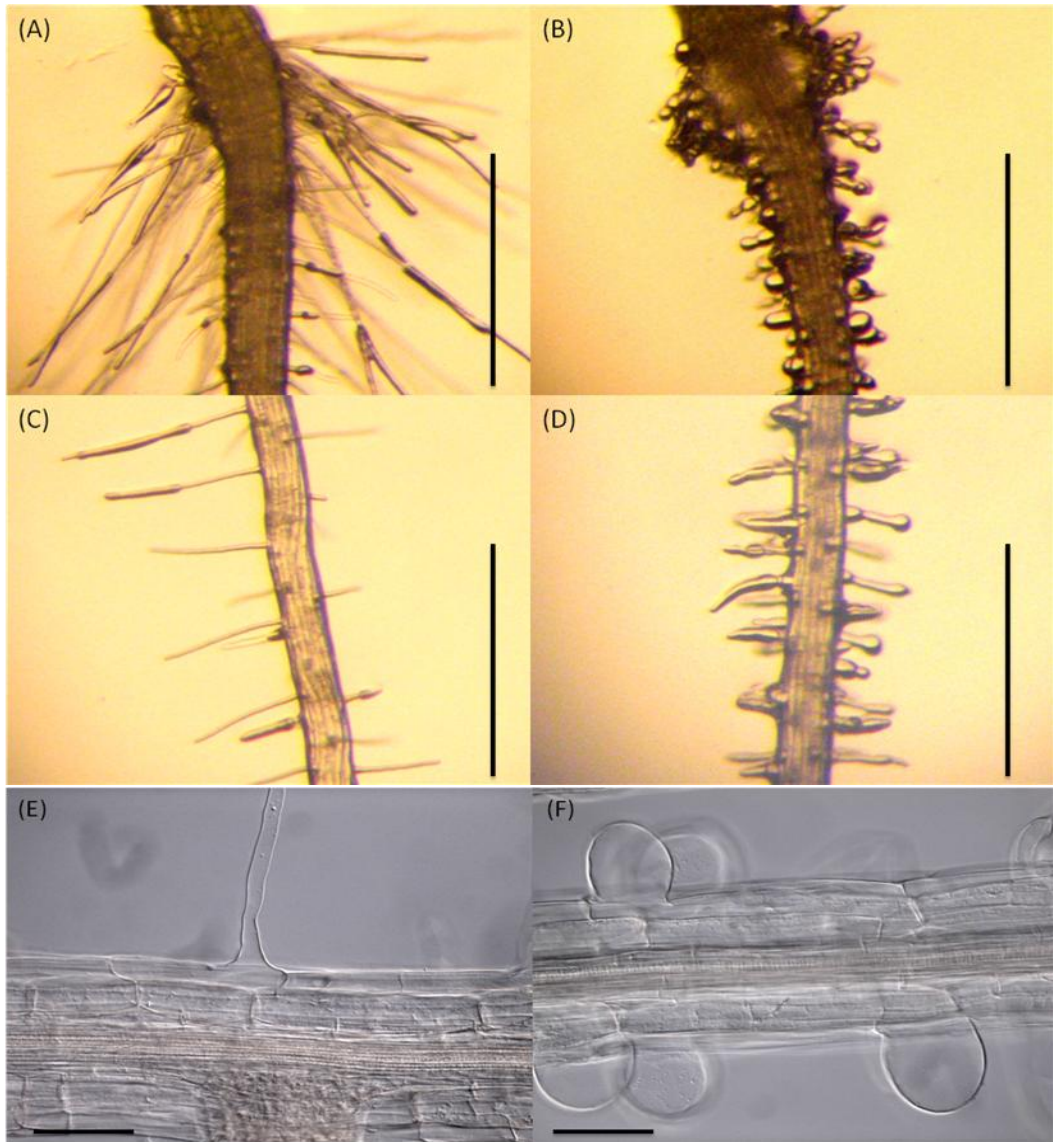
Figure 4.16 Phenotypic analysis of the roots of wild type (A, C and E) and *35S:G2* plant (B, D and F). The 7 day old *Arabidopsis thaliana* primary roots were analysed under the microscope. **Scale bar**: A, B, C, and D: 500 µm. E, F: 50 µm

Based on the morphological differences, the phenotypes of 35S:G2 root hairs were classified into three types: type I, II, and III (Figure 4.17). Type I root hairs, which locate furthest from elongation zone, are extremely swollen. The degree of swelling varies with some trichoblasts being

completely swollen while some were relatively unaffected. No tip growth or elongation was detected in type I hairs. Type II hairs were normally located between type I and type III hairs. Tip growth and elongation was detected but the hairs were much shorter than wild type. The diameters of the hairs varied along the length of the hairs and extra bulges were formed during the elongation process. Type III hairs were located near the root elongation zone and the length was longer than type II hairs but shorter than wild type. Type III hairs should be distinguished from type II hairs by that the diameters of the type III hairs are consistent along the length. Branches were detected in some type III hairs. Some type III hairs also displayed a crooked appearance (Figure 4.17).
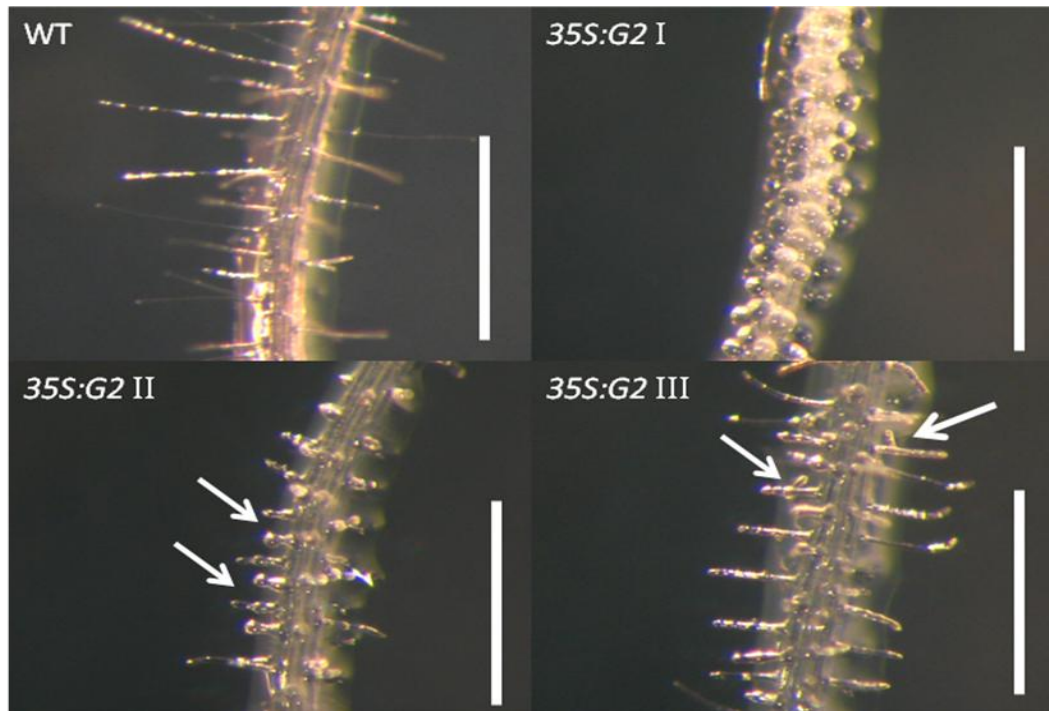
Figure 4.17 Phenotype of wild type and *35S:G2* root hairs. 7 day old *Arabidopsis* roots were analysed under the microscope. WT: wild type. I, II, III: type I, type II and type III. Arrows in 35S:G2 II show the hairs with diameters varied along the length of the hairs. Arrows in 35S:G2 III show the hairs with branches. Scale bar: 500 µm.

Thirty 5-day-old root hairs from two *35S:G2* T3 lines were selected and root hair diameter, length and hair density were measured under a microscope. The same number of 5-day-old wild type seedlings was used for the control. A bar chart describing the average diameter of the three types of root hairs is shown below. The average diameters of *35S:G2* type I, II and III root hairs were 43.73 µm, 28.02 µm and 18.40 µm compared to 10.19 µm in wild type (Figure 4.18).
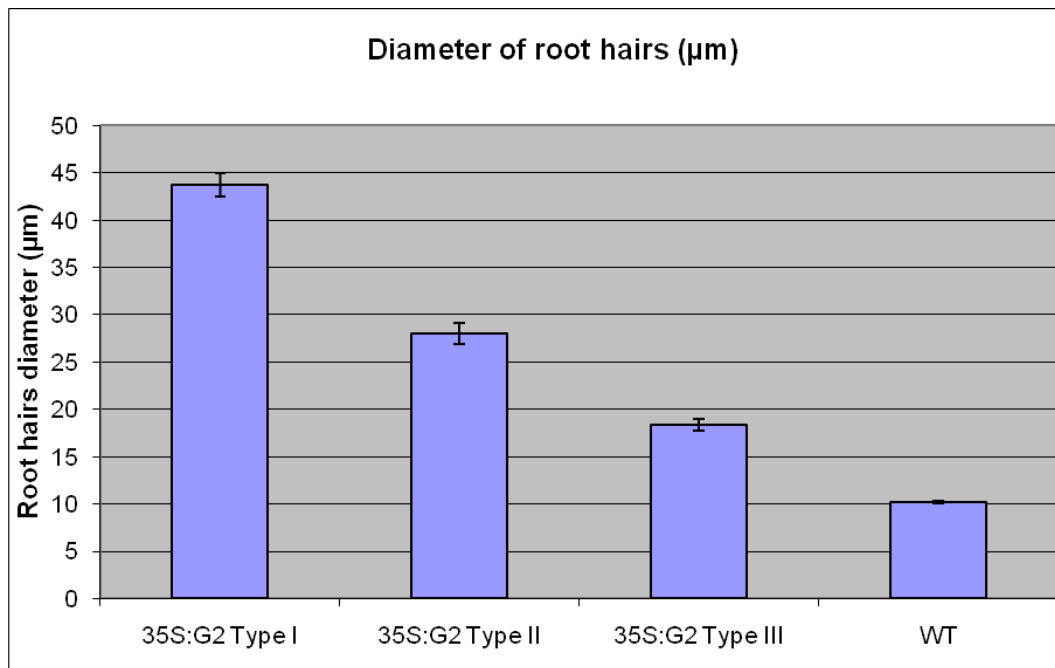
Figure 4.18 The diameters of *35S:G2* type I, type II and type III root hairs. The diameters were determined by calculating the average diameter of thirty root hairs. Error bar: stand error.

The average length of *35S:G2* type I, II and III root hairs was 37.90 μm, 82.42 μm and 298.53 μm compared to 424.00 μm in wild type (Figure). The average length of type I hairs was lower than 40 μm, which indicates that there was no tip growth in type I hairs (Figure 4.19).
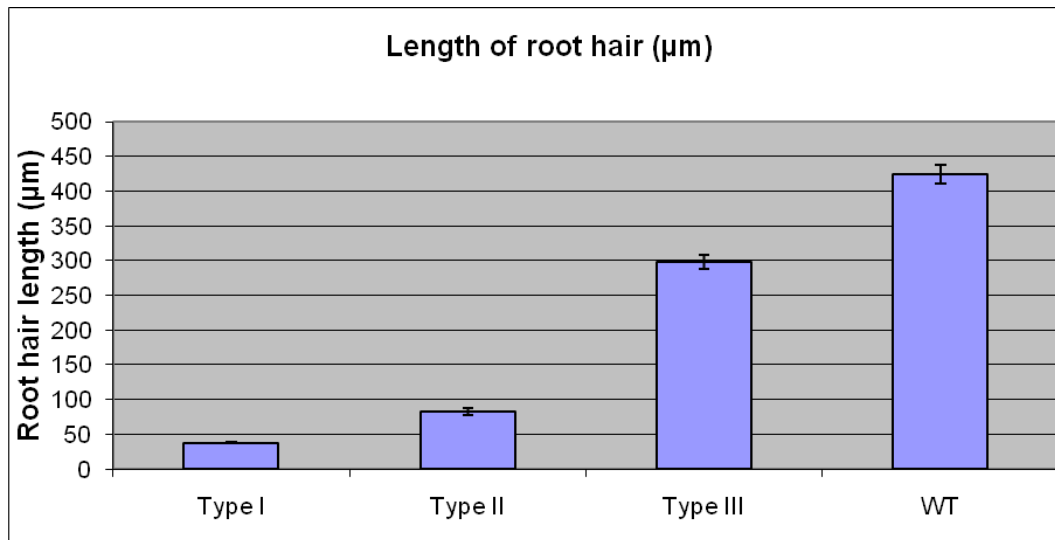
Figure 4.19 The length of *35S:G2* type I, type II and type III root hairs. The length was determined by calculating the average length of thirty root hairs. Error bars: standard error.

The density of root hairs was measured by counting the quantity of root hairs per 1 mm in the elongation zone of roots. The value was determined by calculating the average number per 1 mm of twenty root hairs. *35S:G2* seedlings were shown to have 19.35 root hairs per 1 mm, which was 0.75 greater than wild type (18.6 per 1 mm) (Figure 4.20).
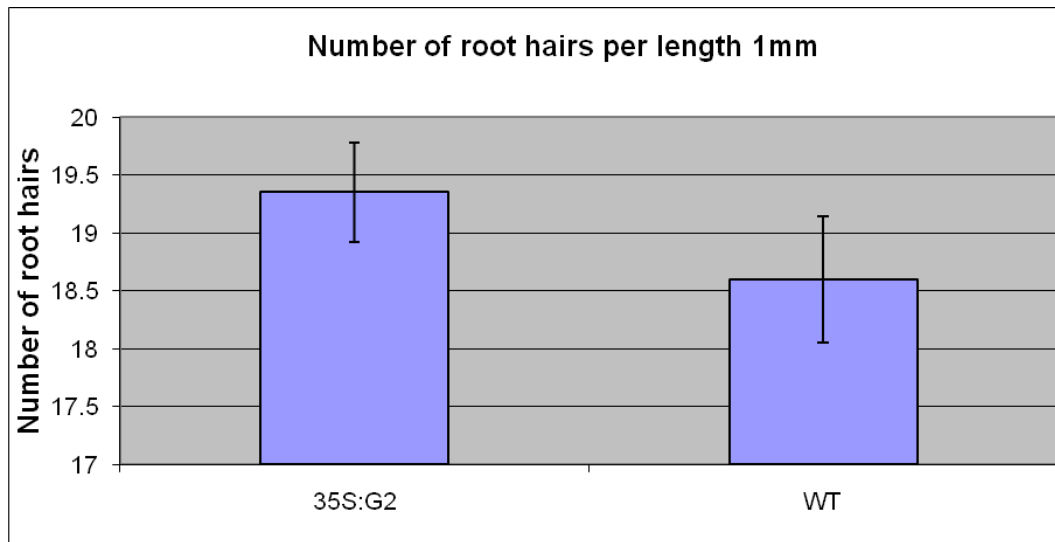
Figure 4.20 The density of *35S:G2* and wild type root hairs in the elongation zone. The density was determined by calculating the average number per 1 mm of twenty root hairs. Error bars: Standard error.

4.3 Crossing *35S:G2* with *35S:IDA*

In chapter 3 it was demonstrated that *G2* is an abscission-related gene on the basis of expression analysis. A gene expression manipulation strategy was carried out in order to investigate the function of *G2*. However neither down-regulating nor up-regulating the expression of *G2* has revealed a phenotype modified in the floral organ abscission.

The expression analysis of *G2* discussed in chapter 3 revealed a negative correlation between *G2* and *INFLORESCENCE DEFICIENT IN ABSCISSION* (*IDA)* which is an important abscission-related gene*.* It has been shown that *IDA* controls floral organ abscission and the null mutant without the presence of IDA fails to shed its floral organs (Butenko *et al.,* 2003). Further analysis of plants with ectopically expressed *IDA* showed that such material had an earlier abscission and exhibited an extended AZ (Stenvik *et al.,* 2006). *35S:IDA* plants were also associated with enhanced production of arabinogalactan protein (AGP). This was substantially secreted in the AZ and the amount secreted was much more than that found in wild type. AGP was absent in the AZ of *ida* (Stenvik *et al.,* 2006). Further expression analysis by micro array and RT-PCR showed that one of the AGPs in *Arabidopsis, AGP24* was up-regulated in *35S:IDA* and down-regulated in *ida* (Stenvik *et al.,* 2006)*. IDA* is not only expressed specifically in the AZ but also in the cortex and epidermal cells overlying lateral root primordial and a mutation in *IDA* also leads to a delay in lateral root emergence (Kumpf *et al.* 2010).

G2 and *IDA* have a similar expression patterning with both of them expressing in AZ and in the cortical cells adjacent to emerging lateral roots and both of them are strongly up-regulated by IAA. Expression analysis showed a negative correlation between *G2* and *IDA.* Given the above observation, a cross between *35S:G2* and *35S:IDA* was performed in order to further investigate the interactions between *G2* and *IDA.*

4.3.1 Screening and isolation of homozygous lines of *35S:G2 × 35S:IDA*

To investigate the potential relationship between *G2* and *IDA,* a cross was carried out between *35S:G2* and *35S:IDA*. As both *35S:G2* and *35S:IDA* are dominant, the genotype can not be characterized by phenotype. In order to select the homozygotes, genomic PCR screening was carried out to determine the genotype of F2 and F3 progenies. DNA isolated from individual plants was analyzed using 35S-promoter-specific and gene-specific primers. In the F2 generation, individuals with both PCR amplifications of *35S:G2* and *35S:IDA* were selected (Figure 4.21) and F3 lines generated. PCR was performed on F3 lines with at least 24 individuals per line. Lines with 100% individuals having both PCR amplifications from 35S forward and *G2/IDA* specific primers (Table 1.1) were selected as homozygotes. Figure 4.22 shows that the F3 line B13 was homozygous for both genes.
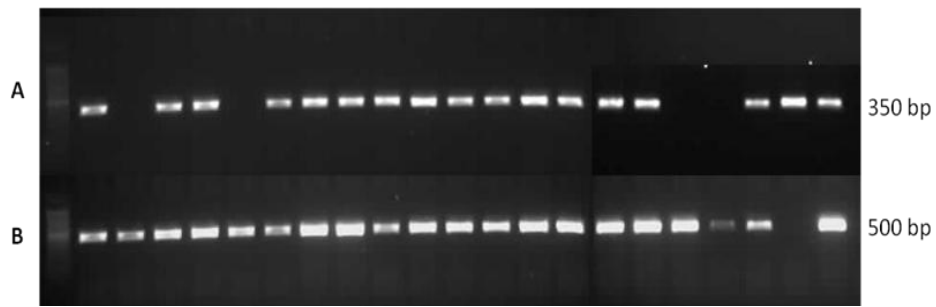
Figure 4.21 Genomic PCR to select F2 generation of *35S:G2* x *35S:IDA*, **Group A** shows the amplification from 35S_Forward and IDA_Reverse primers and **Group B** shows the amplification from 35S_Forward and G2_Reverse primers.
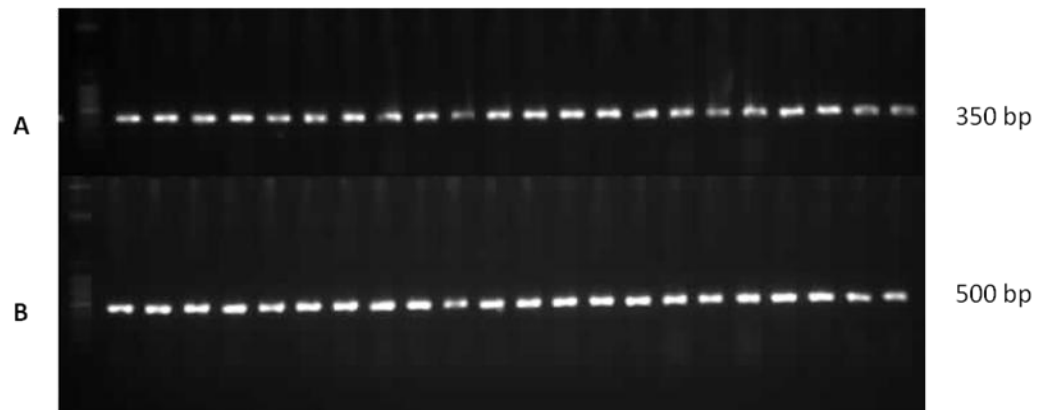
Figure 4.22 Genomic PCR to select F3 homozygotes of *35S:G2 x 35S:IDA* (line B13), Group A shows the amplification from 35S_Forward and IDA_Reverse primers and Group B shows the amplification from 35S_Forward and G2_Reverse primers.

## 4.3.2 Phenotype of *35S:IDA* x *35S:G2* lines

Overexpression of *IDA* leads to a series of phenotypes. Firstly, *35S:IDA* individuals show earlier abscission from position 4 compared to position 6 –

8 of wild type. Secondly, *35S:IDA* plants show an extended abscission zone. Thirdly, a large amount of AGP is secreted at the site of abscission and this is maintained until the silique is mature (Stenvik *et al.*, 2006). *35S:G2* does not show any visible phenotype in floral organ abscission.

An in-depth analysis of floral organ abscission was carried out on *35S:IDA, 35S:G2* and *35S:G2 × 35S:IDA* plants with wild type as control. In terms of the timing of abscission, *35S:IDA* lines showed early abscission at position 3, compared to position 6 in wild type. Both *35S:G2* and *35S:G2 × 35S:IDA* showed abscission at position 6, which is the same as wild type (Figure 4.23). In terms of the development of AZ, *35S:IDA* individuals showed significant extended AZs which were easy to be distinguished, whereas *35S:G2 and 35S:G2 × 35S:IDA* showed no visible difference from wild type (Figure 4.24).
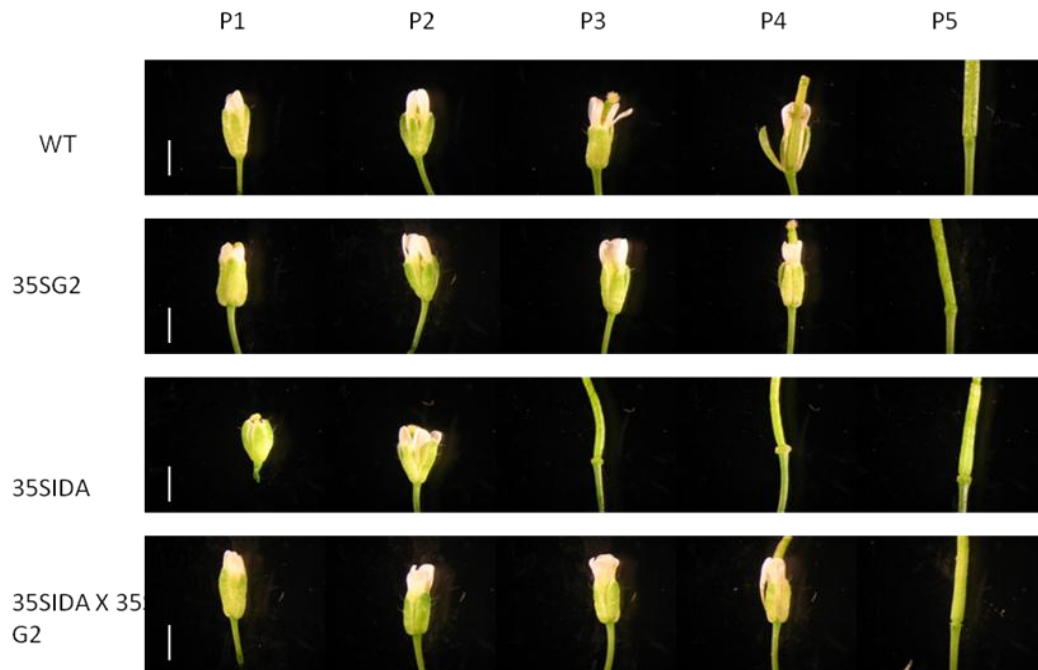
Figure 4.23 Time course analysis of floral organ abscission of wild type (WT), *35S:G2, 35S:IDA* and *35S:IDA x 35S:G2* plants. The shedding position was analyzed by gentle shaking of the flowers. **P**: position. **Scale bar:** 1 mm.
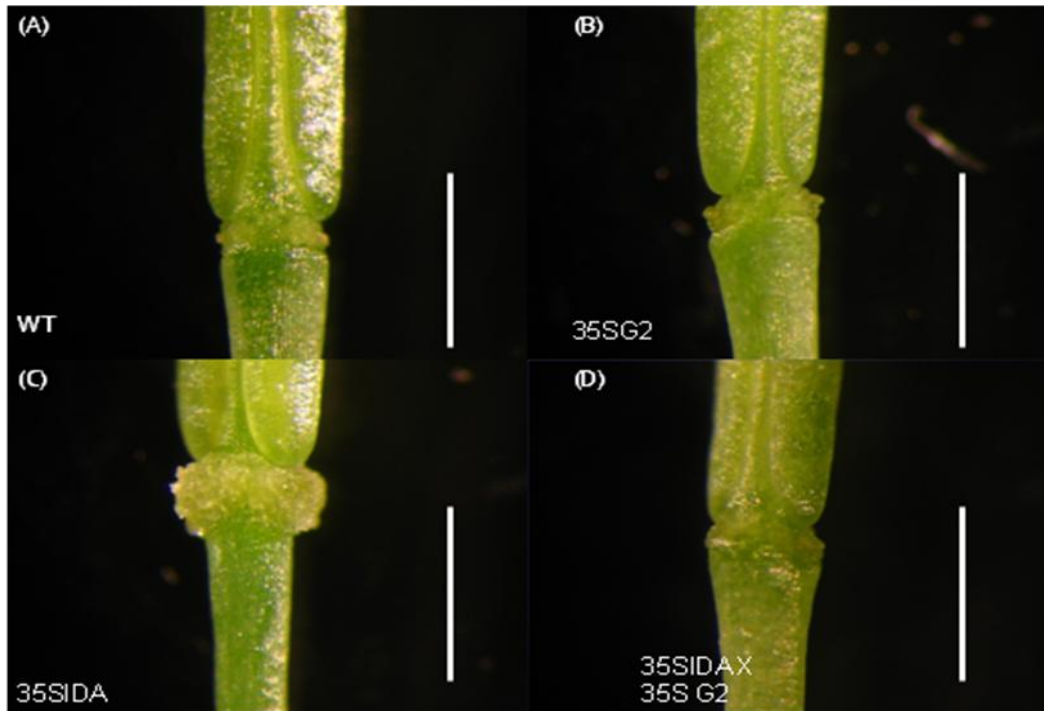
Figure 4.24 Floral AZ of wild type (WT) **(A)**, *35S:G2* **(B),** *35S:IDA* **(C)** and *35S:IDA x 35S:G2* **(D).** *35S:IDA* shows a significantly extended AZ and with white material covering the AZ whereas *35S:G2 and 35S:IDA x 35S:G2* show no difference from wild type. Scale bar: 500 µm.

In terms of the secreted AGP, in *35S:IDA* a white substance (AGP) was detected covering the extended AZ. No white substance was detected either in *35S:G2* or *35S:G2 × 35S:IDA*, which was the same as the wild type. A synthetic chemical reagent β-D-glucosyl Yariv (β-GlcY) was used to determine production of AGP. *35S:IDA* showed a higher amount of AGP covering the AZ whereas in wild type only a small amount of AGP was detected at position 4. Interestingly, no AGP or less AGP was detected in both *35S:G2* and *35S:G2 x 35S:IDA* plants (Figure 4.25)*.*

These results reveal that by overexpressing *G2* in a *35S:IDA* background, in terms of floral organ abscission and AZ development, the phenotypic characteristics are lost and *35S:IDA* x *35S:G2* plants look essentially like wild type. The series of effects indicate that overexpression of *G2* can rescue *35S:IDA* phenotypes. This observation suggests that *G2* and *IDA* could function in the same pathway or that expression of *IDA* is down-regulated by *G2*.
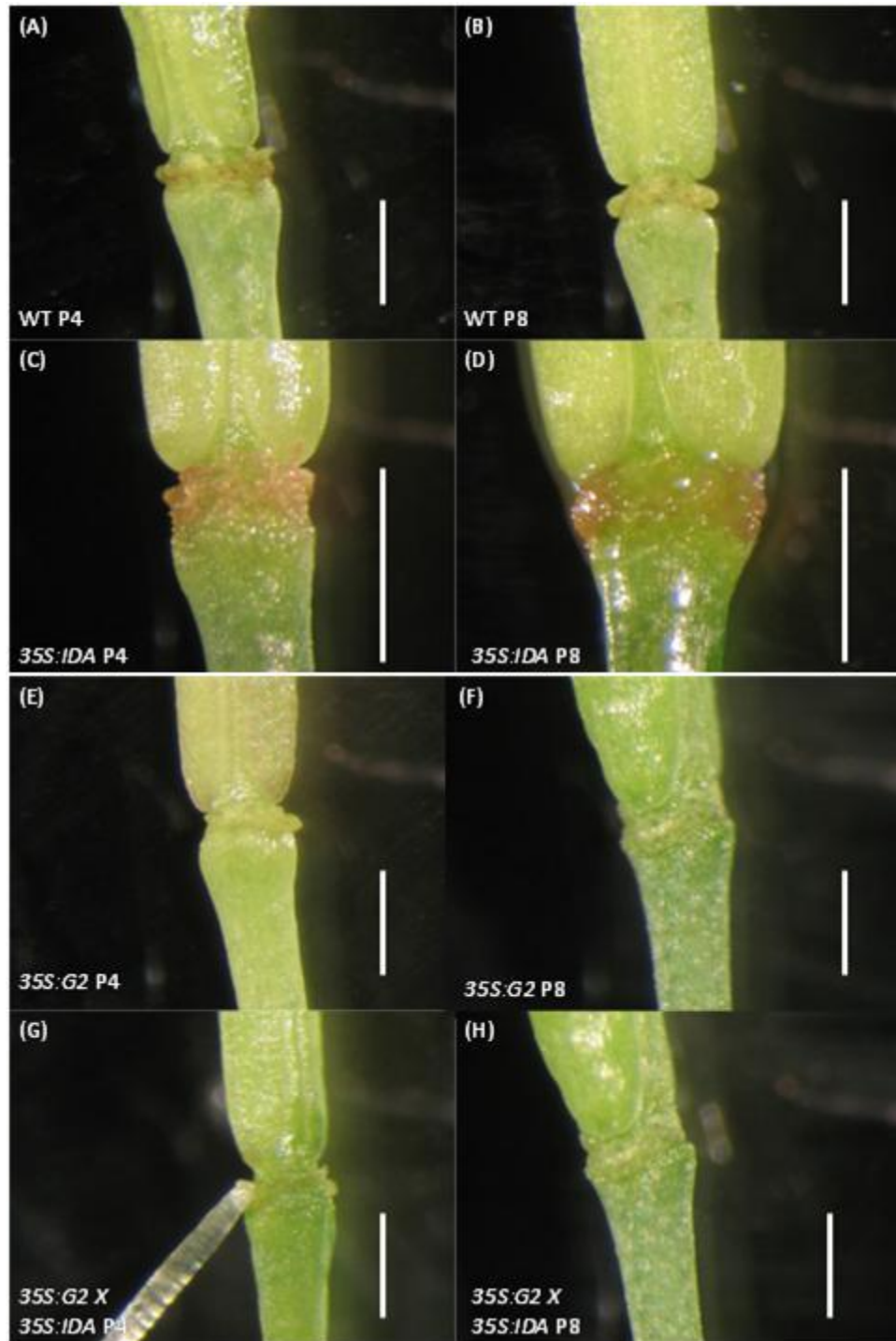
Figure 4.25. Identification of Arabinogalactan using the Yariv Reagent β-GlcY. Staining areas are shown in red. **(A, B)** wild type (WT), **(C, D)** *35S:IDA,* **(E,F)** *35S:G2,* **(G,H)** *35S:G2 x 35S:IDA.* **(A, C, D, E)** were selected from position 4 (P4) and **(B, D, F, H)** were selected from position 8 (P8). Scale bar: 500 μm.

To test the hypothesis that *IDA* is down-regulated by *G2*, a quantitative-Reverse Transcription-PCR (qPCR) was performed to determine the expression pattern of *G2* and *IDA* respectively in the backgrounds of *35S:G2, 35S:IDA, 35SG2 × 35S:IDA*, and wild type, following the protocol which was described in chapter 2.2.7. Total RNA was isolated from both flowers (P5 – P8) and cauline leaves. Two biological duplicates and two independent samples from each duplicate were examined. The relative expression levels were normalized to the expression of *ACTIN – 2 (ACT2).* The qRT-PCR results showed that *G2* expression was significantly up-regulated in the *35S:G2* plant compared to wild type whereas in the *35S:IDA* background *G2* expression was observed to be very slightly down-regulated. The *G2* expression in the background *35S:G2 × 35S:IDA* was unaffected compared to the wild type but the expression in the flowers of *35S:G2 × 35S:IDA* plants was slightly lower than in *35S:G2* background, which suggests that the up-regulation of *IDA* in a *35S:G2* background down-regulated *G2. IDA* expression was detected in the flowers of the *35S:G2* and wild type backgrounds and the expression was up-regulated in the *35S:IDA* background. Compared to the expression in both the flowers and cauline leaves of *35S:IDA, IDA* expression in the *35S:G2 × 35S:IDA* background was found to be slightly down-regulated, suggesting that over-expression of *IDA* is down-regulated by ectopic expression of *G2* (Figure 4.26)*.* However the observed expression changes were very slight and further experimentation is required to determine if they reflect biologically significant expression changes.

A

G2		35S:G2F	35S:G2L	35S:IDAF	35S:IDAL	x F	x L	WTF	WTL
IDA									
ACT2									

B

G2 expression in different backgrounds

Expression level

| 35SG2F | 35SG2L | 35SIDAF | 35SIDAL | XF | XL | WTF | WTL |

C

IDA expression in different backgrounds

Expression level

| 35SG2F | 35SG2L | 35SIDAF | 35SIDAL | XF | XL | WTF | WTL |
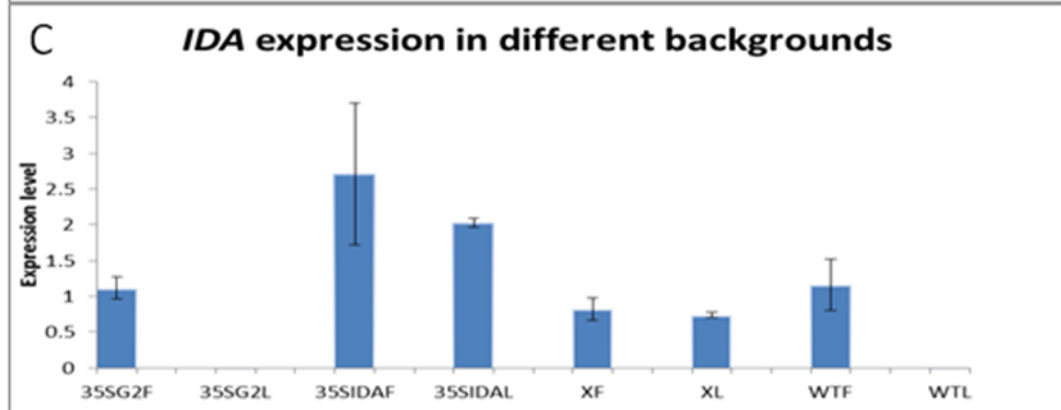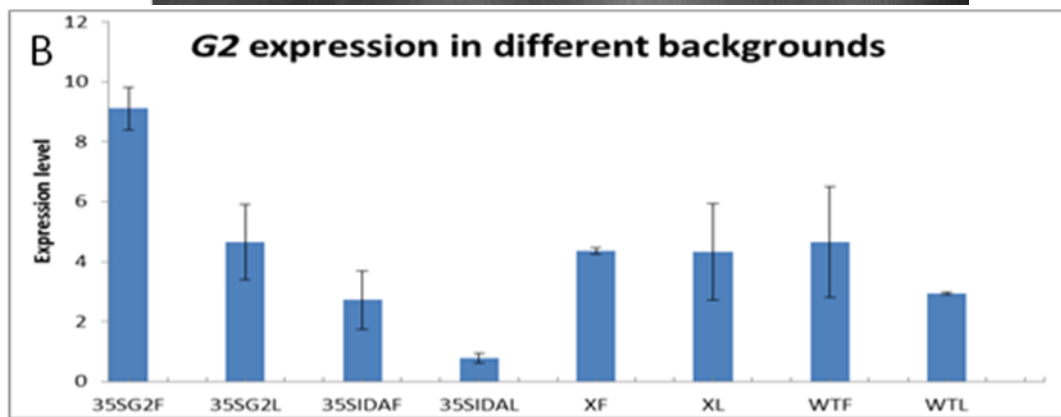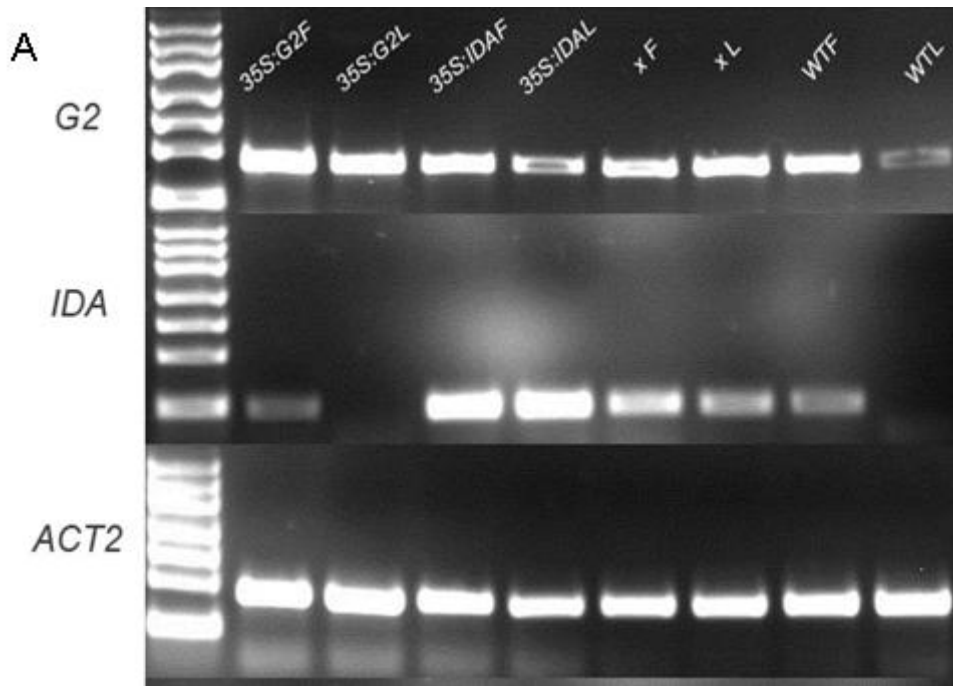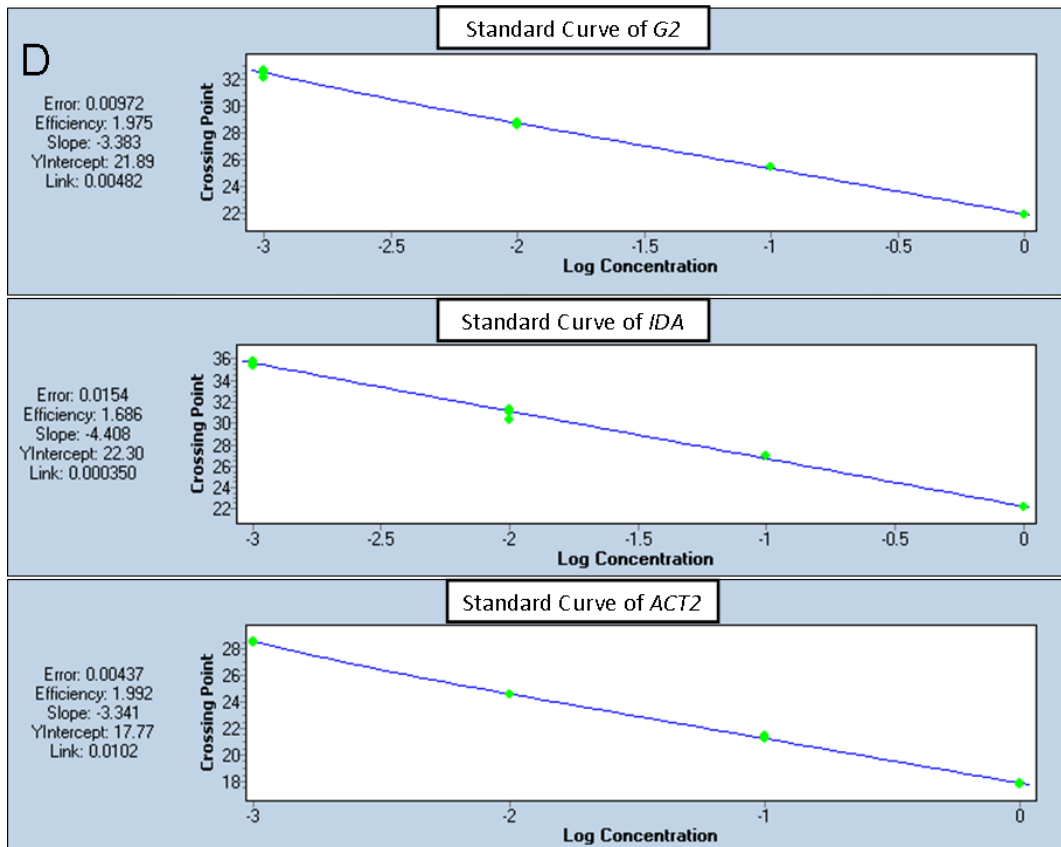
Figure 4.26: qRT-PCR of mRNA from both flowers (F) (P5 – P8) and cauline leaves (L) of *35S:G2*, *35S:IDA*, *35S:IDA x 35S:G2* (x) and wild type. A: RT-PCR result before qRT-PCR performed. B: qRT-PCR result of *G2* expression in different backgrounds. C: qRT-PCR result of IDA expression in different backgrounds. D: Standard curves of *G2* (efficiency 1.975), *IDA* (efficiency 1.686) and *ACT2* (efficiency 1.992). Error bar: Stand error.

4.3.3 *35S:IDA x 35S:G2* homozygous plants were observed to be normal in morphology and development compared to *35S:IDA.*

Apart from the morphological and developmental changes in floral organ AZ, *35S:IDA* also showed other phenotypic characteristics. Vestigial AZs were found at the bases of pedicels, branches and cauline leaves (Stenvik *et al.*, 2006). In addition, *35S:IDA* plants are significantly smaller in structure. In most of the *35S:IDA* plants rosette leaves were observed to senesce more rapidly.

As described in the previous sections, *35S:G2* plants showed no significant difference compared to wild type except in the phenotype of root hairs. *35S:G2* x *35S:IDA* homozygous plants showed no visible difference comparing to wild type, which indicated that the non-abscission-related effects of overexpression of *IDA* are also rescued by *35S:G2* (Figure 4.27).
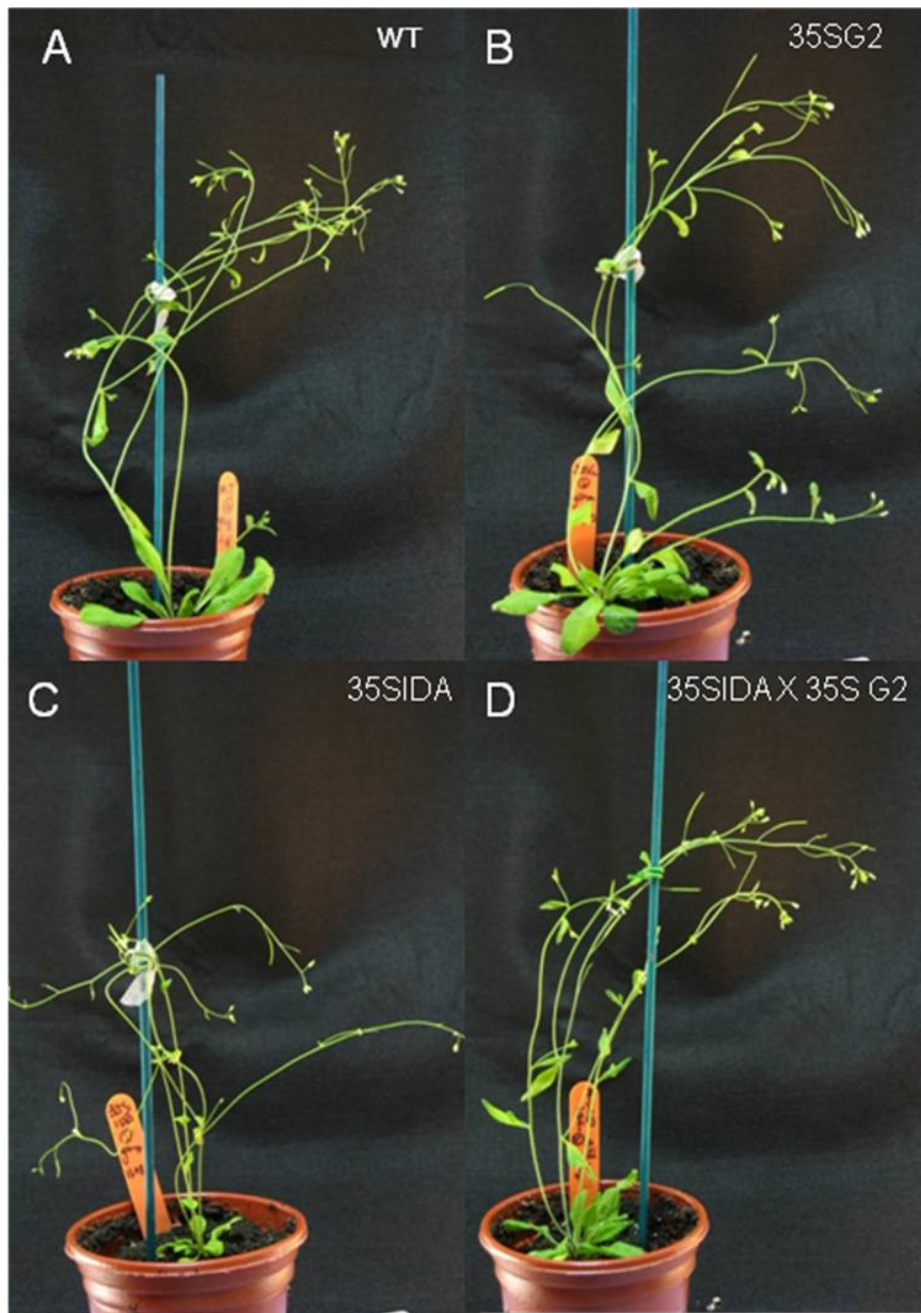
Figure 4.27 Phenotypes of whole plants of **A** wild type (WT), **B** *35S:G2*, **C** *35S:IDA* and **D** *35S:IDA* x *35S:G2.*

4.3.4 *35S:IDA* rescues the phenotype of swelling root hairs of *35S:G2*

As the result that has been described in chapter 3, overexpression of *G2* leads to a phenotype of root hair swelling. In *35S:IDA x 35S:G2* homozygous plants the phenotype of extremely swollen root hair was not observed, while shorter and branched hairs were detected, which indicated that *35S:IDA* rescues the root hairs bugling effect of type I hairs but not type II and type III hairs (Figure 4.25).
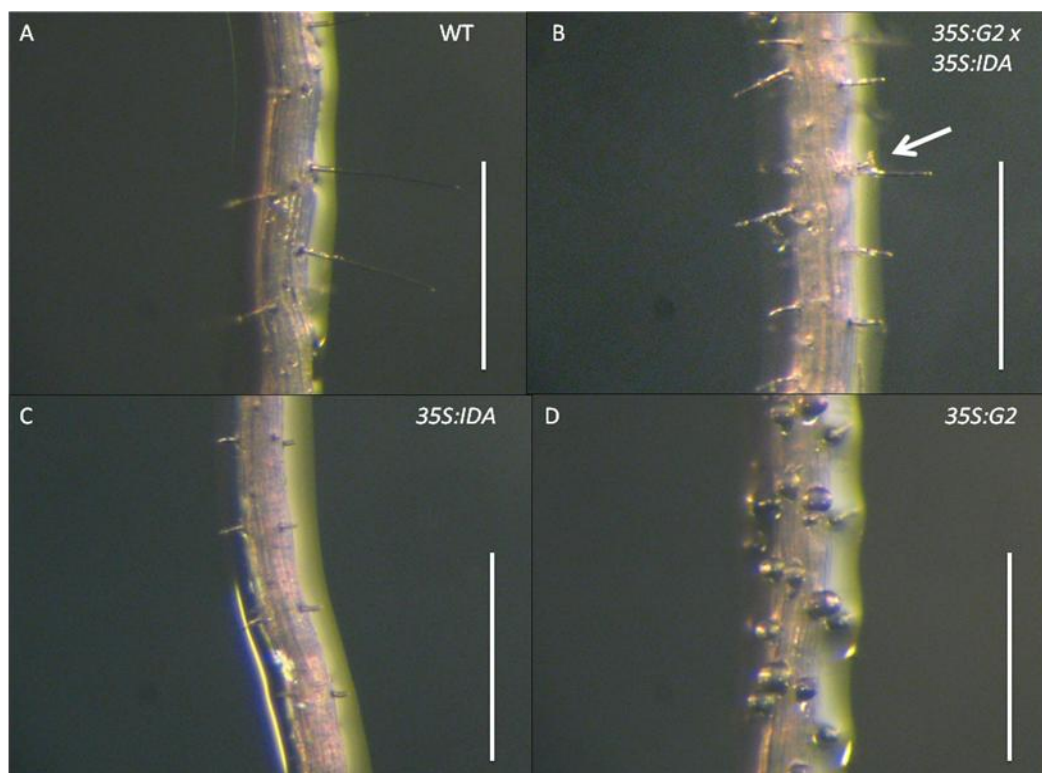
Figure 4.28 *Arabidopsis* root hairs. **A:** wild type (WT). **B:** *35S:G2* x *35S:IDA*. **C:** *35S:IDA*. **D:** *35S:G2*. The arrow shows the branched root hair in *35S:G2 x 35S:IDA* plant. Scale bar: 500 µm

35S:IDA plants showed significant smaller seedlings and rosette leaves than wild type while *35S:G2* plants showed no difference. Interestingly, compared to wild type, *35S:G2* and *35S:IDA,* the *35S:G2 x 35S:IDA* homozygotes showed a different rosette leaf morphology with a decrease in width and increase in length which is consistent even until the plant becomes mature, while the size of the whole seedling was similar compared to wild type (Figure 4.29). 30 leaves from 21-day-old seedlings of *35S:G2 x 35S:IDA, 35S:G2, 35S:IDA* and wild type were isolated and measured for the leaf length to width ratio. The results showed that the ratio of leaf length to width were wild type: 2.12, *35S:G2:* 2.14, *35S:IDA:* 1.93 and *35S:G2 x 35S:IDA:* 3.09, which suggested that *35S:G2 x 35S:IDA* plants developed a different rosette leaf morphology.

Figure 4.29 The morphology of rosette leaves (**Group A**: whole seedlings, **Group B**: rosette leaves from the same position). WT: wild type.

4.3.5 Immunolocalization of *35S:G2* root hairs

It has been shown that the amount of AGP secretion in AZ is reduced in *35S:G2* comparing to both *35S:IDA* and the wild type. AGPs were predicted to act as a mediator between the cell wall and cortical microtubules in *Arabidopsis* root tissue and the absence of AGP leads to swollen root hairs by disrupting the microtubules (MT) (Andeme-Onzighi *et al.,* 2002), therefore it is possible that the down-regulatation of AGP in *35S:G2* root hairs may lead to the phenotype of swollen root hairs. In order to investigate if the MT structure was changed in root hairs, an immunolocalization strategy was applied to localize MT.

The immunolocalization was carried out as shown in chapter 2.2.19 using 5-day-seedlings of *35S:G2* and wild type plants. Antibody Antitublin (Abnova^{TM}) was used as primary antibody and antibody Anti-rabbit IgG (Abnova^{TM}) was used as the secondary antibody. The results are shown in figure 4.30.
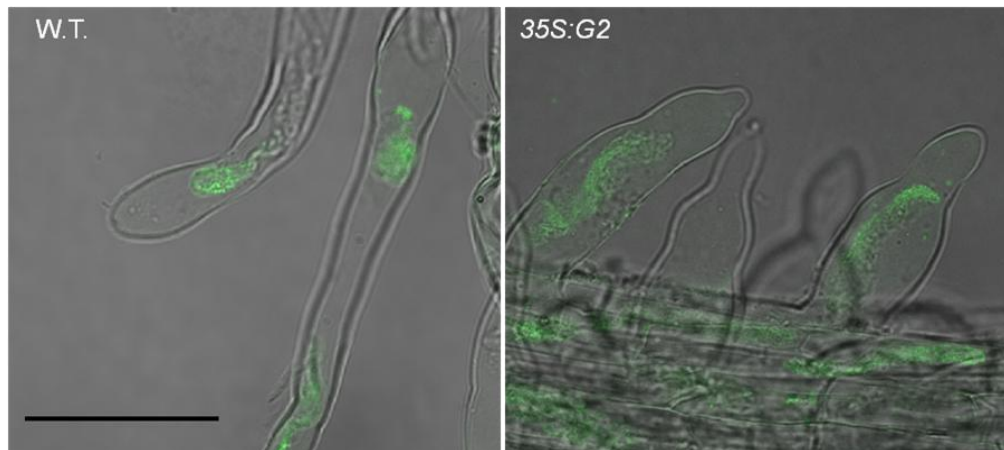
Figure 4.30: Immunolocalization of the microtubules (MTs) in root hair cells of wild type (W.T.) and *35S:G2.* MTs are stained in Green

Figure 4.30 shows that the MT could be visualized using this technique but that the internal structure of the root hairs was disrupted and appeared to be "shrunk". The reason could be that in this analysis, the fixing system for the tissue was not suitable for fixing root hairs. In a future study methods such as freeze substitution could be applied to overcome this issue.

4.3.6 Generation of a translational fusion by fusing G2 protein with GFP.

In order to localize G2 protein at a cellular level, G2 protein was fused with the GFP marker. Fragments with 1841 base pairs covering the full length of *G2* cDNA and 1504 base paris of promoter area, were fused into an entry vector pDONR221 (Invitrogen™) by using a Gateway™ Technology (Figure 4.5). Because the gene does not have an intron, primers with attB1.1 and attB2.1 sites were designed and the amplified fragments from PCR by using

Phusion^{TM} DNA Polymerase were purified before fusing them into the vector pDONR221 by the Gateway^{TM} BP-reaction strategy which was described in section 2.2.10. The resulting construct was called PrG2Entry (Figure 4.31). The plasmids were then transformed into E.*coli* strain DH5α using a heat-shock method (Sambrook *et al.,* 1989) as described in section 2.2.8**.** The transformed cells were selected by spreading the cells on LB medium plates containing 50 µg/ml kanamycin and the resistant plasmids were isolated and purified using a NucleoSpin^{TM} Plasmid mini kit which has been described in section 2.2.9. The plasmids were confirmed by PCR (Figure 4.32) and then sent for sequencing.
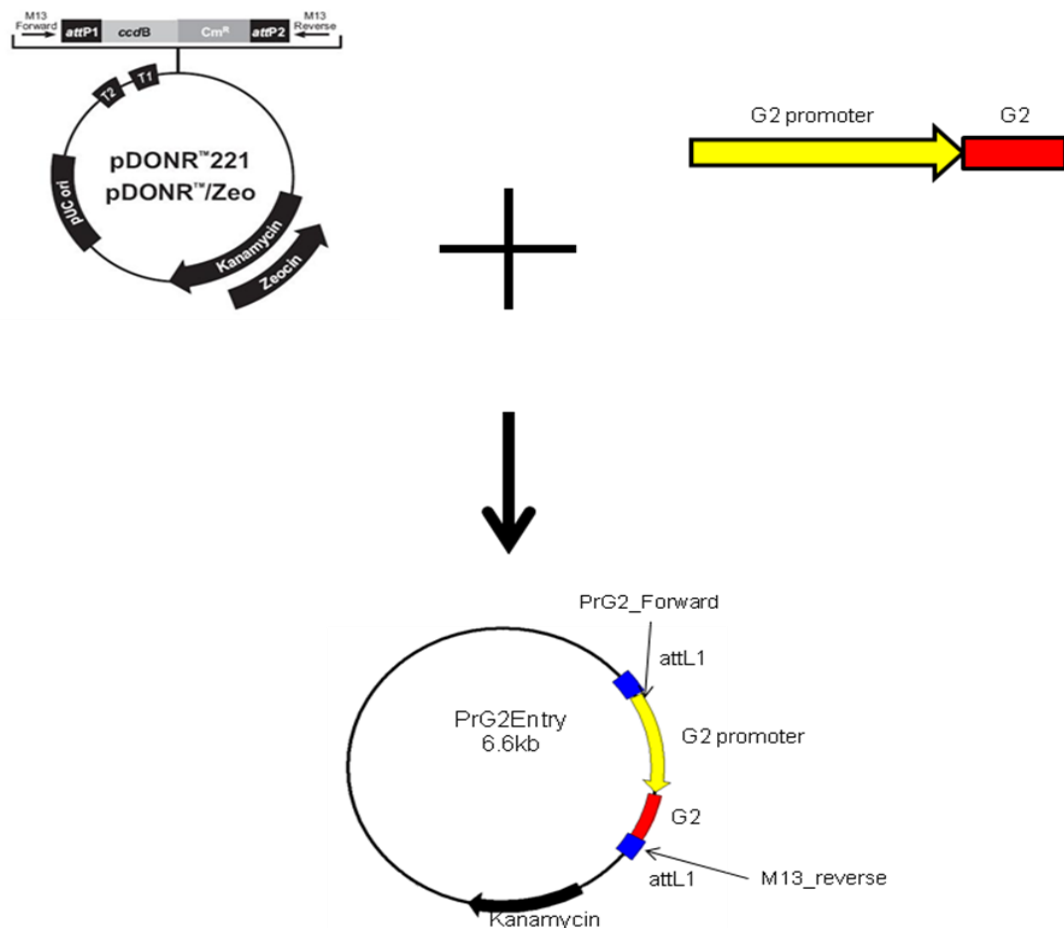
Figure 4.31: Schematic diagram of G2Entry plasmid construct. The 1841 bp *G2* genomic DNA insert was fused into pDONR^{TM}221 by BP reaction. A kanamycin-resistance gene was used as a selectable marker in bacteria. The diagrams are not drawn to scale.
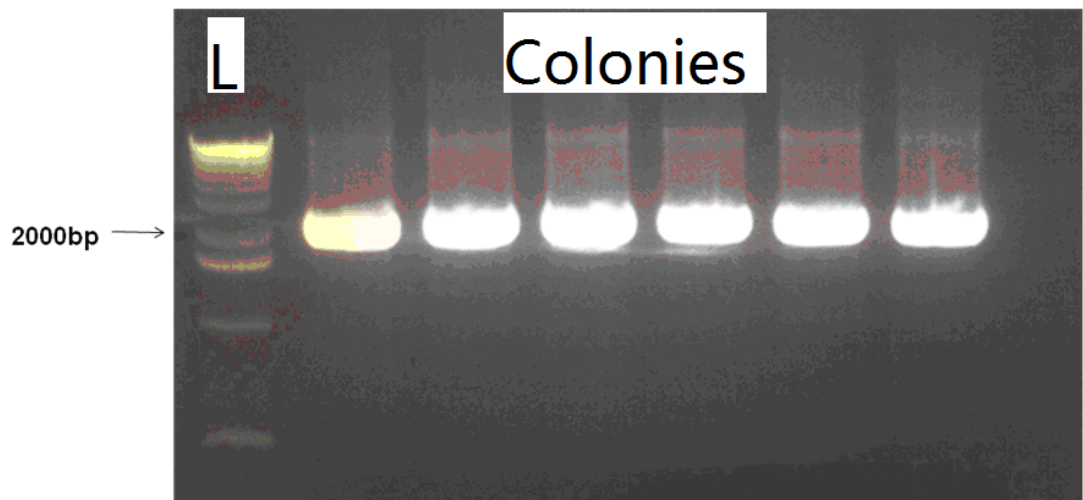
Figure 4.32: PCR analysis of the colonies that contain the PrG2Entry plasmid using primers

PrG2_Forward and M13_reverse. The positions of the primers are shown in figure 4.27. L: ladder.

The full length fragment was then inserted into a destination vector pGWB4 which was described in section 2.1.2. The Gateway^{TM} technology LR reaction was then carried out following the procedure described in section 2.2.10. To confirm that transformation was successful, a genomic PCR was carried out using G2_forward primer and GFP_reverse primer and a band with expected size was obtained. The final construct was named *prG2:pGWB4*. A diagrammatic representation of the construct is shown in Figure 4.33. Prior to the transformation, the constructs both in *E.coli* DH5α and *Agrobacterium tumefaciens* C58 were confirmed by PCR using specific primers. Bands of the expected size were successfully amplified (Figure 4.34).
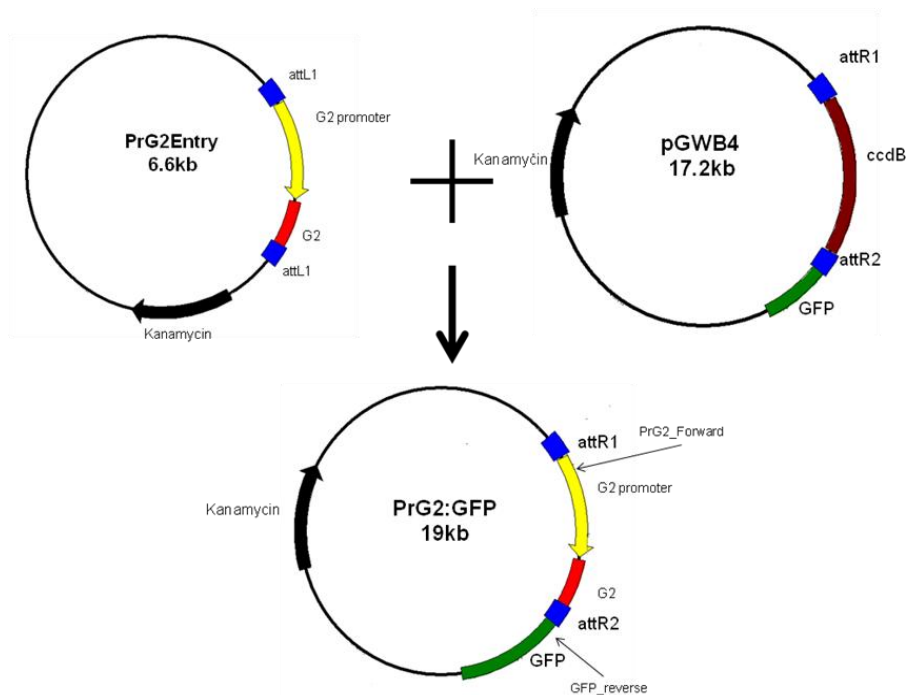
Figure 4.33: The fragment in the Entry Clone PrG2Entry was transferred to a destination vector, pGWB4, which contains compatible recombination sites, attR1 and AttR2, in a reaction mediated by GatewayTM LR ClonaseTM Enzyme Mix (Invitrogen). The resulting construct was named PrG2:GFP. This construct is expected to fuse the GFP marker at the C terminal of G2 protein therefore to locate G2 protein in the cellular level. The diagrams are not drawn to scale.
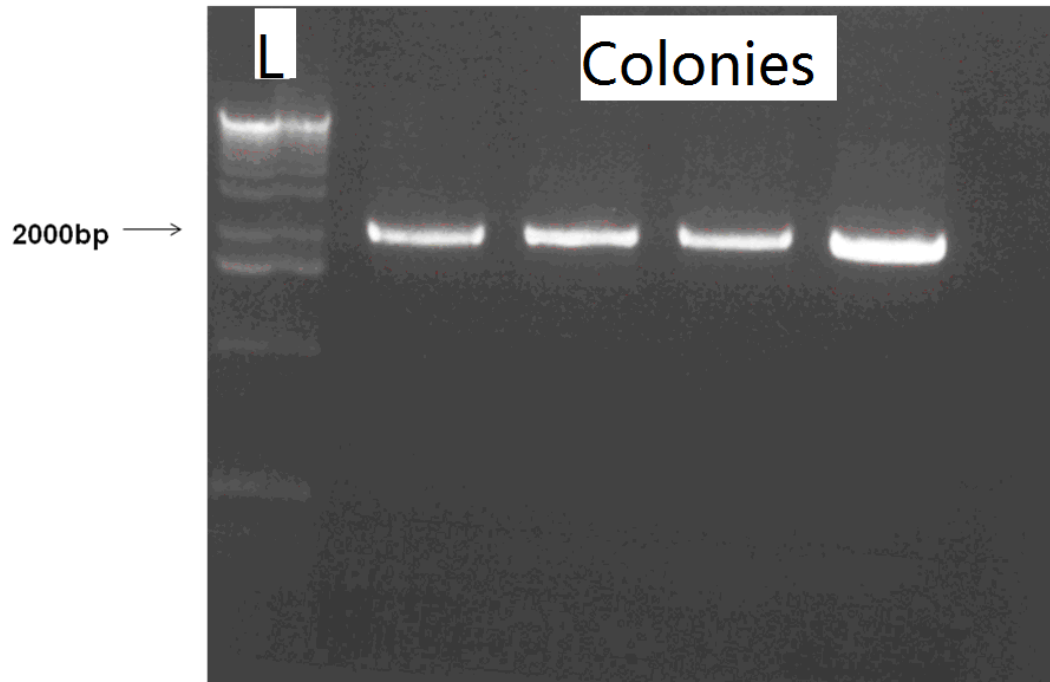
Figure 4.34 PCR analysis of plasmids from the 4 colonies of transformed *Agrobacterium tumefaciens* C58. L: ladder. PCR products were amplified using primers PrG2_Forward & GFP_reverse. The position of primers is shown in Figure 4.29.

PrG2:GFP were obtained and transferred into pots containing Levington M3 compost and GFP expression examined during floral organ shedding. However no GFP signal was identified. The reason for this could be that the fusion of G2 protein and GFP disrupt the GFP structure so that no GFP signal could be visualised. To solve this issue, in a future study the GFP protein could be placed at the N terminal of the G2 protein. However, apart from antibiotic selection, there was no further confirmation (eg, genomic PCR, sequencing or expression analysis) to show that the construct was successfully transferred into the plants, therefore future studies, are needed to confirm the nature of the problems encountered.

4.4 Discussion

4.4.1 Generation and analysis of lines down-regulated in the expression of *G2.*

An insertional mutagenesis strategy was pursued to obtain KO lines of *G2.* The insertions were located 310 bp or 360 bp upstream of the translation start site. Although homozygous lines were isolated, RT-PCR results indicated that *G2* expression was not affected by the insertion. The reason could be that both of the SALK line T-DNA insertions were located in *G2* promoter area and the insertions did not disrupt the transcription initiation. No T-DNA insertion line was available in the exon region of *G2* from the database searching (http://www.arabidopsis.org). Therefore an RNAi strategy was designed and implemented in order to knock down *G2* expression. Two homozygous lines were confirmed by RT-PCR to be silenced.

A phenotypic consequence of silencing *G2* was found in developing pods. Seeds from the transgenic line were observed to be aborted in mature siliques of the *RNAi:G2* homozygous plants compared to wild type under normal growing conditions. Statistical analysis in the development rate of seeds showed that only 25% of visible seed in siliques developed in siliques of *RNAi:G2* lines compared to 92% in wild type. Study of the morphology of the undeveloped seeds indicated that the ovules were failed to develop. Genevestor_V3 showed that *G2* was expressed in ovary and the level of

expression was "medium", which suggested that *G2* could play a role in ovary development. Interestingly, some pollen grains were found to be undeveloped in *RNAi:G2* plants. *G2* is expressed in the stamen in accordance with Genevestor_V3 data, suggesting that the gene may be involved in pollen development.

G2 may be functional redundant with one or more of the other 9 genes in abscission process (chapter 3), which could also be the reason of that no abscission-related phenotype was detected in *G2* null lines. The gene *At1g10530,* which is predicted by Genevestigator_V3 that it is expressed specifically in AZ with a medium level of expression, could be functional redundant with *G2.* To test this hypothesis, a double-KO of *G2* and *At1g10530* could be generated and the abscission properties of the material studied.

4.4.2 Overexpression of *G2* in *35S:IDA* background rescues the effects of *35S:IDA* in floral organ abscission

G2 has been shown to be expressed highly in AZ (Chapter 3). However no significant difference was observed in either the KO line or the overexpression line in terms of floral organ abscission comparing to wild type. Firstly, no abscission-related phenotype was detected in *RNAi:G2* lines. The bioinformatics analysis described in chapter 3 revealed nine proteins in *Arabidopsis* that shared domain I and III with G2 and both of the domains were predicted to be potentially responsible for the function of G2. These genes could form a new family in *Arabidopsis* and be functionally redundant with G2, which could be the reason why there was no phenotype in mutants with the absence of G2. Another explanation is that G2 could be involved in the protection process against pathogens on cell wall synthesis, so that no physical phenotype could be detected. Secondly, no abscission-related phenotype was observed in *35S:G2* plants. The reporter gene and RT-PCR analysis showed that the expression level of *G2* was high and exceeded the threshold in AZ in a wild type background, therefore overexpression of *G2* might not make a significant difference.

The expression analysis of *G2* which has been described in chapter 3 has shown an inverse correlation between *IDA* and *G2* with the wounding induced *G2:GUS* signal down-regulated by the overexpression of *IDA. IDA*

has been reported to play an important role in regulating floral organ abscission and absence of *IDA* leads to partial degradation of the middle lamella and an inhibition of abscission (Butenko *et al.* 2003). Overexpression of *IDA* leads to a series of phenotypes including early abscission, extended AZ development and secreted AGP. These features are easy to distinguish from the wild type (Stenvik *et al.,* 2006), whereas in *35S:G2* plants no change in either the timing of abscission or the development of the AZ was observed. To further investigate the relation between *G2* and *IDA,* a cross between *35S:G2* and *35S:IDA* was carried out.

Homozygotes of *35S:G2* x *35S:IDA* were selected by PCR using 35S_Forward and G2/IDA_reverse primers (Table 1.1). The timing of abscission and the development of AZ were examined in the *35S:G2 x 35S:IDA* homozygotes and the result showed that *35S:G2 x 35S:IDA* homozygous plants did not exhibit the *35S:IDA* phenotype. This observation suggests that overexpression of *G2* can rescue the effects of *35S:IDA* in terms of floral organ abscission. Compared to the wild type, homozygous plants did not show either an earlier abscission or an extended AZ region. In addition, vestigial AZs were not found at the bases of pedicels, branches in *35S:IDA* x *35S:G2* plants and the partial shedding of siliques was also not observed. Finally, the plants retained a wild type size and appeared to be much "healthier" than *35S:IDA* plants. The above observations indicate that overexpression of *G2* rescues the effects of *35S:IDA.* The RT-PCR result suggests that when ectopically expressed *G2*

is introduced into a *35S:IDA* background, overexpressed *IDA* is down-regulated and the amount of expression of *IDA* was similar as in wild type background. This could be the reason why the *35S:G2 x 35S:IDA* homozygote did not show a *35S:IDA* phenotype.

Interestingly, no, or a lower amount of AGPs was detected in *35S:G2* and *35S:G2 x 35S:IDA* background compared to that observed in a *35S:IDA* background. *AGP24* was reported to be up-regulated in *35S:IDA* plant and absent in *ida* mutant background (Stenvik *et al.,* 2006). The function of AGPs in the abscission process is unknown but there are reports showing that AGPs may be involved in molecular interactions and cellular signalling (Showalter, 2001). In addition, AGPs were predicted to act as a mediator between the cell wall and cortical microtubules in *Arabidopsis* root tissue (Andeme-Onzighi *et al.,* 2002). Whether AGPs are involved in the similar process during abscission remains unknown, however it would be worthwhile investigating microtubule orientation during abscission which could be achieved by an immunolocalization strategy.

Leaves of the rosette leaf of the *35S:G2 x 35S:IDA* cross display a reduction in width compared to wild type and this phenotype is prolonged until the plant becomes mature. This effect can not be detected in either *35S:G2* or *35S:IDA* plants. In addition, *35S:IDA* can partially recover the phenotype of the swollen root hairs in *35S:G2* (this observation will be discussed in the following sections), indicating that *35S:G2* can not fully

suppress the *35S:IDA* phenotype. The RT-PCR analysis shows that *G2* and *IDA* expression in *35S:G2* x *35S:IDA* plants are down-regulated compared to *35S:G2* and *35S:IDA* pants. This could be one of the reasons that the cross has a unique morphology of its rosette leaves.

## 4.4.3 Overexpression of *G2* leads to swollen root hairs

The overexpression lines of *G2* were obtained by fusing *G2* cDNA with a 35SCaMV promoter. RT-PCR was performed in order to confirm the ectopic expression of *35S:G2*.

The *35S:G2* root hair was classified into three types based on the morphology. Type I hairs were extremely swollen and failed to transfer to tip growth. Type II hairs were short and vary in diameter along their length. Type III hairs were not only short but also crooked and display branches. Rachel and Dolan (2002) separated root hair development into four phases: (1) the specification of hair-producing cells; (2) the initiation of root hair growth; (3) tip growth and elongation; and (4) cessation of mature root hairs growth. In plants with ectopic expression of *G2,* the position and amount of root hairs was not affected, which indicates a change in the morphology of root hairs occurs under the impact of *35S:G2* and that the transfer to tip growth and the tip growth/elongation process is disrupted. Cellulose

microfibrils have been shown to control the direction of expansion (Green, 1962) and the deposition of microfibrils is believed to be under the control of the cytoskeleton (Heath & Seagull, 1982). Microtubule cytoskeleton has been reported to control the tip-growth of root hairs (Heath & Seagull 1982, Sieberer 2005). The mutant *root epidermal bulger 1 (reb1-1)* (Andeme-Onzighi *et al.*, 2002) shows a similar phenotype to type I hairs in *35S:G2* plants with bulging trichoblasts and this has been shown to be accompanied by disrupted cortical microtubules. This mutant has been shown to lack arabinogalactan-protein (AGP). Although attempts to investigate the microtubules in root hairs using an immunolocalzation strategy were not successful, it is possible that overexpression of G2 leads to a loss of arabinogalactan-protein which could result in the bulging of root hairs.

G2 may play a role in interaction with IDA and IDL genes

In *35S:IDA* plants, secreted AGPs were detected and this process was blocked by overexpressing *G2*. Our staining results with the chemical reagent β-GlcY on *35S:G2* and *35S:G2 x 35S:IDA* flowers showed that less AGPs were detected compared to the wild type in the AZ. RT-PCR results showed that overexpression of *G2* resulted in a down-regulation of *IDA* and down-regulation of *IDA* leads to the absence of AGP in AZ. This AGP has been shown to be AGP24 (Stenvik *et al.* 2006). *AGP24* is most highly expressed in pollen and highly expressed in root hair zone, endodermis and cortex, according to Genevestigator_V3 data (https://www.genevestigator.com/gv/) (Figure 4.35).
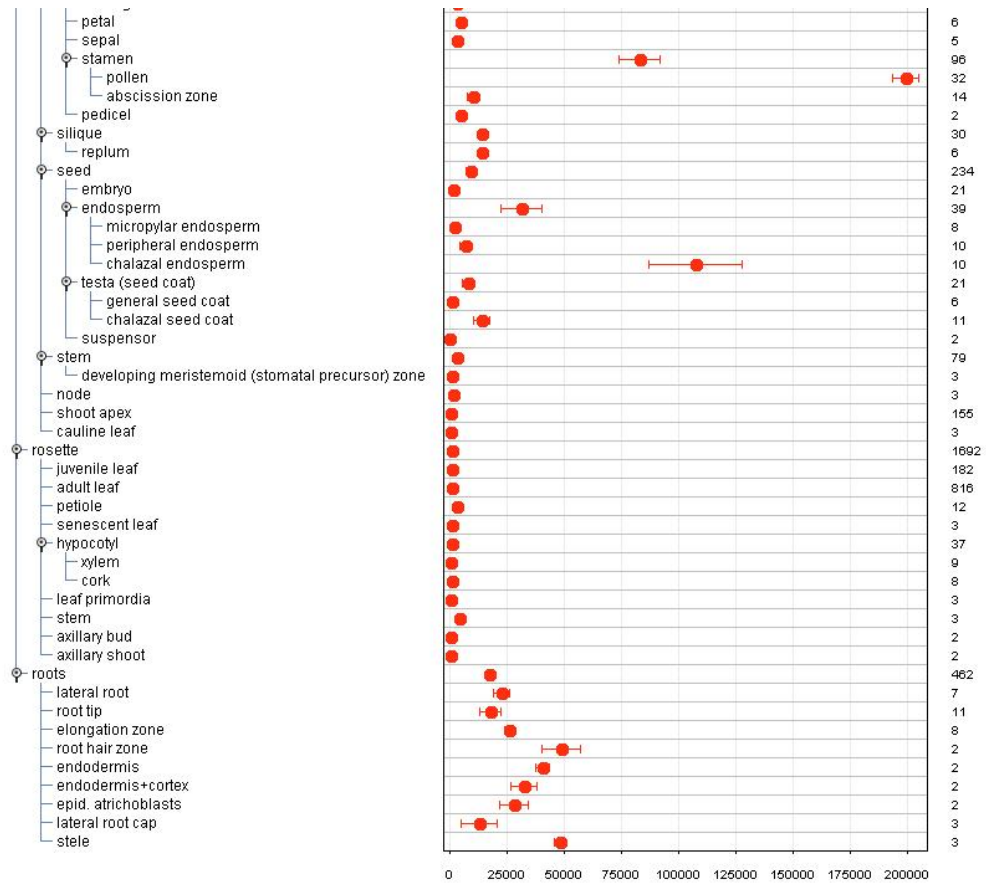
Figure 4.35 Genevestigator V3 result of the expression value of *AGP24* in tissues of *Arabidopsis*.

AGPs have been reported to mediate interactions between the cell wall and cortical microtubules and the mutation of *root epidermal bulger 1-1 (reb1-1)* leads to a reduction of AGP in root, and a disruption of cortical microtubules which results in a bugling of trichoblasts (Andeme-Onzighi *et al.* 2002). It has been shown in chapter 3 that there is a negative correlation between the expression of *G2* and *IDA* and the RT-PCR result presented in this chapter suggests that *IDA* is down-regulated by ectopically expressed *G2*.

Overexpression of *G2* leads to bulging root hairs and a hypothesis to account for this may be a change in microtubule orientation. Given the evidence that *IDA* promotes secretion of AGPs and *G2* down-regulates *IDA,* it is possible that the bulging of root hairs in *35S:G2* could be consequence of down-regulating *IDA,* which results in the absence of *AGP* in roots and a disruption in microtubule organisation.

In the 21st International Conference on *Arabidopsis* Research, Kumpf *et al.* (2010) showed that *IDA* played an important role in lateral root (LR) development despite the Genevestigator_V3 data suggesting a low expression of *IDA* in *Arabidopsis* root tissues (data not shown). The absence of *IDA* leads to a delay in lateral development (Kumpf *et al.*, 2010). *IDA* has been shown to be auxin-induced and expressed in cortical cells overlying the primordial (Kumpf *et al.*, 2010), and both of the features are shared with *G2.* However, in terms of root hair development, *IDA* is not expressed in epidermal cells and based on our observation, the *IDA* knock out mutants do not show a swelling in the root hairs, therefore it is not clear that the swelling of root hairs effect in *35S:G2* might be caused by a down-regulation of *IDA.*

IDA encodes a novel family of putative ligands and in *Arabidopsis* there are 5 *IDA* like genes *IDA-LIKE 1 (AtIDL1)* to *AtIDL5* (Butenko *et al.*, 2003)*.* Further analysis has shown that the effect of mutating *IDA* could be largely rescued in plants with *AtIDL1* fused to the *IDA* promoter (Stenvik *et al.*,

2008). *AtIDL1* is strongly expressed in *Arabidopsis* root tissues (Genevestigator data Figure 4.36). Although there has been no report about phenotypic consequences of down-regulating *AtIDL1,* it might be predicted that the absence of *AtIDL1* could lead to a similar effect as overexpression of *G2.*
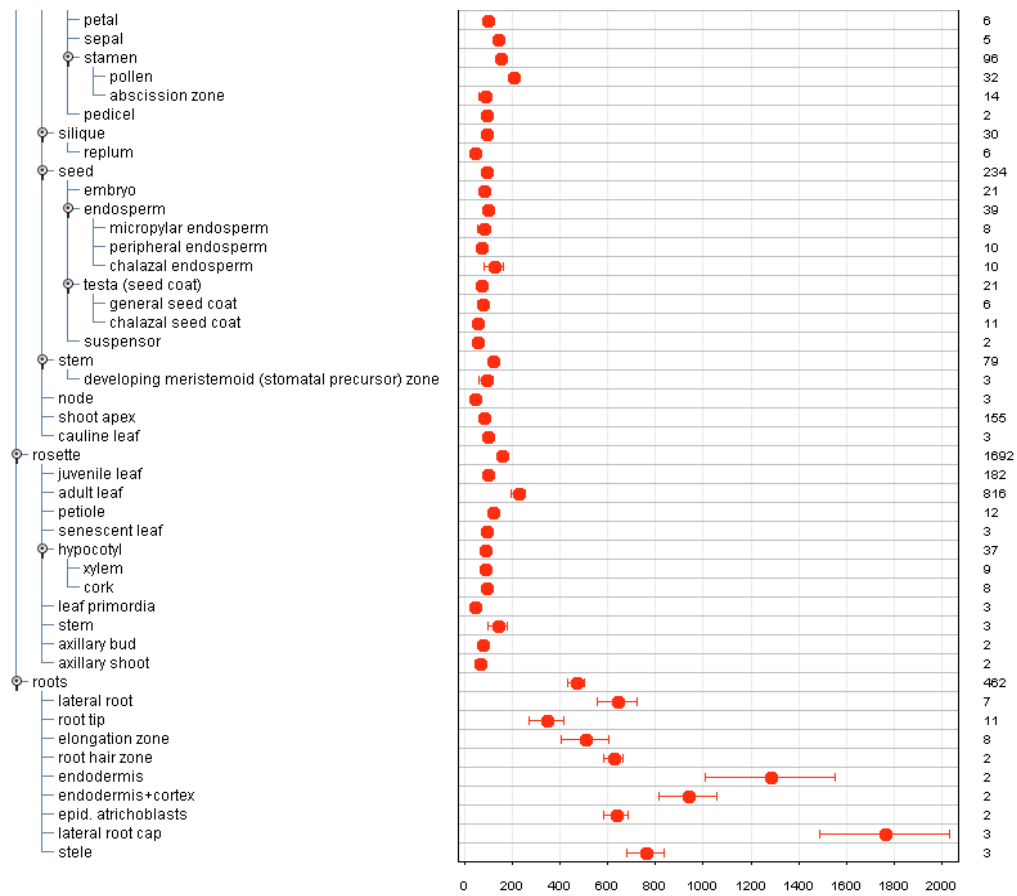
Figure 4.36 Genevestigator result of the expression value of *AtIDL1* in tissues of *Arabidopsis*.

IDA has been reported to be functionally dependent on the presence of the receptor like protein kinase (RLKs) *HAESA* and *HAESA-LIKE2 (HSL2)* (Stenvik *et al.*, 2008). *IDA*, *HAESA* and *HSL2* are functional in the common pathway and IDA and IDL proteins are acting through RLKs in regulating other processes during plant development (Stenvik *et al.*, 2008). However whether *IDL* genes are functional in the same pathway with *HAESA* and *HSL2* is not yet known and there has been no report about the characterization of *IDL* genes.

In addition, the bioinformatic analysis of G2 protein in chapter 3 suggested that G2 could contain a spectrin repeats like domain which acts to bind and interact with other proteins. Therefore it is possible that G2 play a role in binding proteins and involved in the IDA-HAE/HSL2 signalling pathway.

To test this hypothesis, an RT-PCR could be performed to test the expression level of *AtIDL1* in ectopically expressing *G2* lines. Phenotypic analysis could also be carried out on the null lines of *AtIDL1* plants to investigate whether there is change in the morphology of root hair development. Methods such as yeast two-hybrid could also be applied to investigate potential interactions between G2 and IDA/IDL proteins.

The mutant *kojak (kjk)* also fails to transfer to tip growth and hairs become so expanded that they burst at the end (Favery *et al.,* 2001). *KOJAK* was

suggested to be involved in the synthesis of cell wall polymers (Favery *et al.,* 2001). However it is less likely that overexpression of *G2* has an effect on this process for the reasons that type I hairs in *35S:G2* plants do not burst at the end and some of the hairs can successfully transfer to tip growth and elongation.

Overexpression of G2 has an impact on the tip growth process of root hairs

The phenotypic change in the initiation process of root hair development of *35S:G2* was similar to the mutant *reb1-1 (rhd1),* however reports of this mutant have also shown that the total length of the root hair was not affected (Schiefelbein and Somerville, 1990; Andeme-Onzighi *et al.,* 2002). In *35S:G2* plants*,* the disruption of initiation of root hair growth is accompanied by an increase in the diameter of the root hair and a reduction compared to the wild type, suggesting that the process of root hair elongation and tip growth was affected by ectopically expressing *G2*.

In type II hairs of *35S:G2* plants, bulges were observed along the length which causes the hairs to vary in diameter. Type III root hairs show branching and are sometimes crooked. The type II and III hairs are shorter than wild type but exceed the length of 40 µm which suggests that the transfer to tip growth has been successful. Microtubules (MTs) could be a reason for branching and crooked effects. Under normal condition, MTs are longitudinally organized and parallel to the direction of growth of a hair (Baluska *et al.,* 2000; Bibikova *et al.,* 1999). When an *Arabidopsis* root is

treated with MT stabilization drugs, hairs have been shown to be wavy and branched (Bibikova *et al.,* 1999). New growth points were detected on the hair treated with MT stabilization drugs, which suggested that MT could be involved in determination of the apical position of calcium influx (Bibikova *et al.,* 1999). Therefore the disruption of the MTs in *35S:G2* roots could be responsible for the effects observed. Future work might include immunolocalization strategy using anti-tublin as the primary antibody to investigate MT organisation in the *35S:G2* root hairs.

It has been shown that the genes *BST1, CEN1, CEN2, CEN3, RHD3, RHD4, COW1* and *SCN1* play a role in controlling root hair shapes during tip growth (Grierson *et al.,* 1997; Ryan *et al.,* 1998; Galway *et al.,* 1997; Parker *et al.,* 2000). Root hairs in plants without the presence of these genes are short and often altered in morphology (Parker *et al.,* 2000). Mutation of *RHD3* or *RHD4* results in wavy and crooked root hairs (Schiefelbein and Somerville, 1990). Mutation of *CEN1, CEN2* or *CEN3* results in curled root hairs. *bst1* mutants displayed short and straight root hairs which in *scn1* mutants are wide and curled. *rhd3* mutants not only showed short and curled root hairs, but also a shorter root compared to wild type (Schiefelbein and Somerville, 1990). Plants without TIP1 displayed not only shorter root hair but also disrupted pollen tube growth compared to wild type (Schiefelbein *et al.,* 1993). Some root hairs in *35S:G2* roots were observed to be crooked, but no wavy nor curled hair was detected, suggesting that the curve level was much lower than it was in *cen, rhd3.*

It has been shown that mutation of *RHD4, COW1, CEN3* and *SCN1* result in a similar phenotype to the type II and type III hairs identified in *35S:G2* plants. Further work to study the impact of ectopically expressing *G2* could include a series of RT-PCRs to determine the expression of these genes.

When overexpression of *IDA* was introduced into *35S:G2* background, the root hair phenotype was partially recued and no type I hairs were detected, while type II and III hairs were still apparent. An explanation for this observation might be that overexpression of *IDA* leads to the rescuing of AGPs, which rescues the disruption of cortical microtubules. Branched root hairs were sometimes detected in *35S:IDA* roots (Figure 4.37), which suggested that overexpression of *IDA* may also have an impact on the tip growth and the elongation process of root hairs.
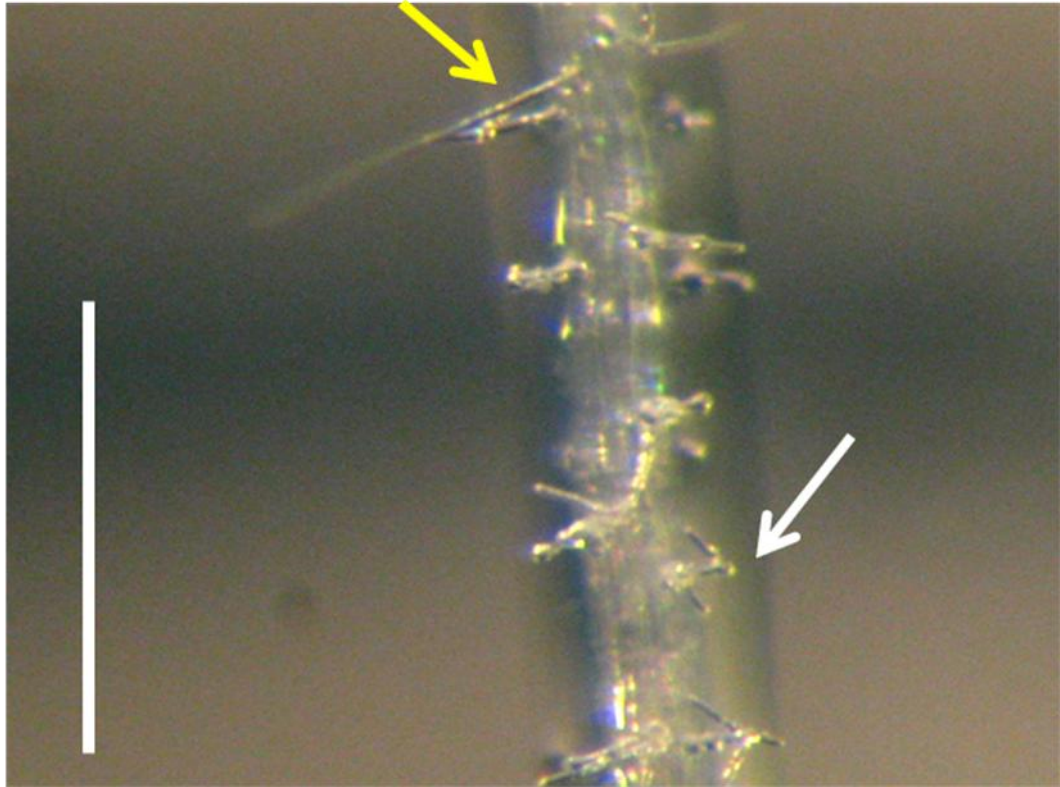
Figure 4.37 Root hair of *35S:IDA* plant. Yellow arrow points to a normally developed hair. White arrow points to a branched hair. Scale bar: 500 μm

During root development, a hair cell is initiated and then a bulge is formed before tip growth and elongation taking place. The two phases are distinct and could be controlled by independent pathways. Ectopic expression of *G2* is likely to disrupt both phases, but whether *35S:G2* achieve this effect through controlling the expression of *IDA* and *IDLs* solely or through other root hair development related genes is unclear.

Given the above information, a predicted model has been developed to describe this potential pathway (Figure 4.38) and future work has been designed to test the predicted model.

Firstly, ectopically expressed *G2* down-regulates *IDA* or *IDLs* (possibly *AtIDL1*) in root, which prevents cortical AGPs from being secreted in the root cortical cells. A lack of cortical AGPs affects cortical and epidermal MTs, which disrupts bulge formation (type I hairs) (Figure 4.38A). To test this hypothesis, the expression of *IDA* and *IDLs* could be quantified by RT-PCR or QPCR using total RNA from root tissue; additionally, a yeast-two-hybrid strategy could be applied to investigate the interaction between *G2* and *IDA/IDLs.*

Secondly, overexpression of *G2* leads to crooked, branched hairs, or hairs forming bulges along the length of the hair (type II and type III hairs). One explanation for this could be that ectopic expression of *G2* disrupts the root hair MTs, which leads to these effects (Figure 4.38B). To test this, an MT could be immunolocalized in roots using an anti-tubulin antibody in wild type and *35S:G2* plants. Overexpression of *G2* may also down-regulates some genes such as *RHD4, COW1, CEN3* and *SCN1* etc, which are critical for root hair development and this might lead to the formation of type II and type III hairs. An RT-PCR or QPCR could be undertaken on root tissue to investigate this possibility.
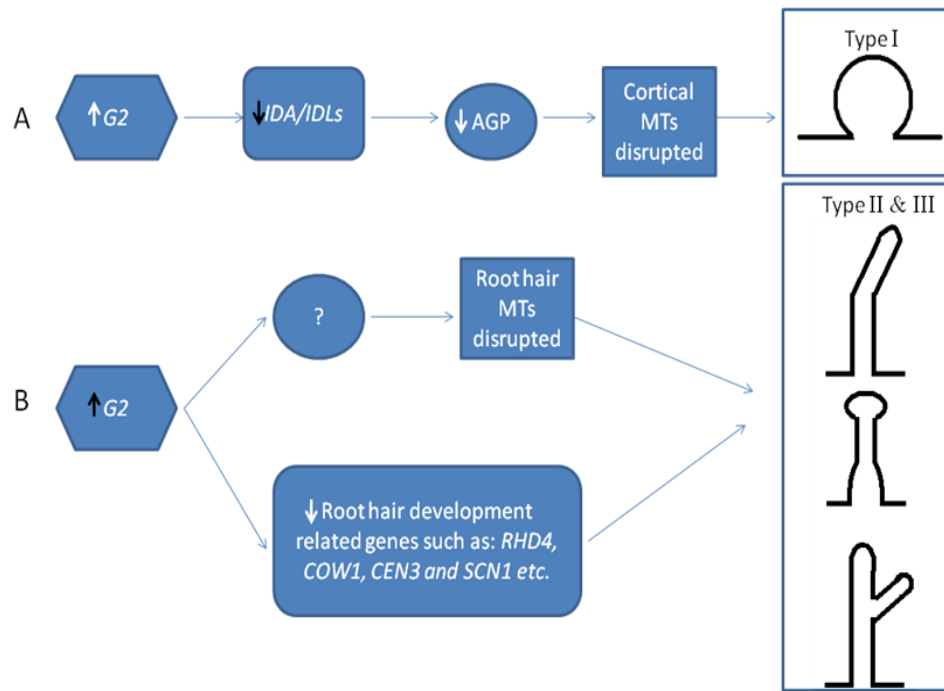
Figure 4.38 Proposed model of how overexpression of G2 leads to the swollen, crooked and branched phenotypes. ↑ suggests the gene is up-regulated and ↓ suggests the gene is down-regulated.